SRI LANKAN GEOTECHNICAL SOCIETY

ANNUAL CONFERENCE

29th September 2011
At the Wimalasurendra Auditorium
Institution of Engineers – Sri Lanka

CONTENTS

Minimization of Rain Induced Slope Failures in Residual Soils

S. A. S. Kulathilaka *, V. Sujeevan, L. M. Kumara

** Professor, Department of Civil Engineering, University of Moratuwa, Sri Lanka*

Abstract : Rain induced failures in slopes made of residual soils are a major geotechnical hazards in Sri Lanka. These soils which are formed by the insitu weathering of the parent rock are characterized by the heterogeneous nature inherited from the difference in mineralogy of the parent rock and the process of variable weathering. Safety margins of these slopes are high during the periods of dry weather due the prevailing matric suctions. Rainwater infiltration causes a loss of matric suction and builds up of positive pore water pressures.

Zones of significantly different; permeability, resistance to erosion and shear strength resulting from variable weathering and the presence of relict joints induce significant complications to the behavior of these slopes. As such, different methods of stabilization and surface protection will have to be adopted within short distances.

The complex nature of such slopes was idealized under three cases and the effect of rainfall on each case was studied. Thereafter, the effectiveness of surface drainage measures such as; sealed berm drains, cascade drains and appropriate slope surface cover in the reduction of negative effects of rainfall was studied. The effect of rainwater infiltration on the pore pressure regime and the effectiveness of the said surface drainage measures were studied using the software SEEPW [4]. The stability of the slopes after a rainfall event was analyzed using the software SLOPEW [3]. The results illustrated that the destabilizing effects of rainfall could be minimized with the usage of appropriate surface drainage and surface protection measures. The need for systematic monitoring to ensure that the stabilizing measures provided are functional is also emphasized.

1. Introduction

Maintaining the slopes in residual soils stable during the periods of heavy rainfall, is a major challenge encountered by Geotechnical and Highway Engineers of Sri Lanka. This challenge has increased in recent times with the need to make deep excavations for the major infrastructure development projects such as Southern Transport Development Project (STDP). In these slopes the degree of weathering can vary in an abrupt manner due to the differences in the mineralogical structure of the parent rock, which is metamorphic. Boundaries of contrasting permeability thus created would cause build up of high pore water pressures and would be detrimental to stability. The presence of relict joints will add to the complexity.

Excessive rainfall is the triggering factor for slope failures under these conditions. It is anticipated that sufficient safety margins could be maintained by minimizing the infiltration of rainwater. In this research, the effectiveness of berm drains, cascade drains and appropriate vegetation cover in minimizing the infiltration was studied. The need to adopt other forms of surface protection measures depending on the nature of the weathered material encountered will also be highlighted.

The study was done for a typical cut slope from the STDP. The water table is low during the periods of dry weather and high matric suctions exists above the ground water table. The matric suction is assumed to increase at a negative gradient to reach a maximum value of 100 kN/m^2. (Figure 1). Prevailing matric suctions enhance the stability of the slope. Infiltration of rainwater causes a depletion of the matric suction and positive pore water pressures could develop as rainfall prolongs.

The complex geological condition of a typical slope was idealized under three cases, namely: a uniform residual soil (case 1), thick layer of residual soil underlain by weathered rock (Case 2) and a thin layer of residual soil underlain by weathered rock (Case 3).

The process of infiltration under the idealized geological conditions was modeled with the software SEEP/W [4]. The resulting pore pressure regime was incorporated in the stability analysis done with the software SLOPE/W [3]. Due to the non uniform nature, both circular and non circular modes of failure were considered.

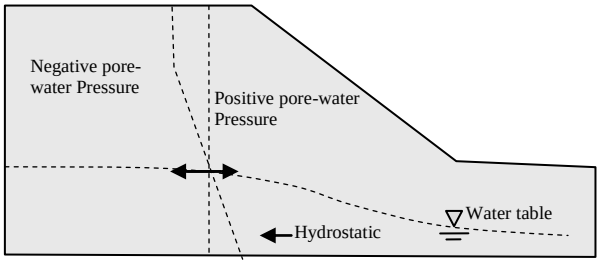

Figure 1– Initial Pore water pressure distribution

2. Hydraulic Properties of Unsaturated Soils

The most fundamentally important feature in the analysis of the behavior of an unsaturated soil is the Soil Water Characteristic Curve (SWCC). It shows the variation of the matric suction with the volumetric water content.

Figure 2 shows an idealized SWCC with two characteristic points A* and B*.Point A* corresponds to the air-entry value ($(u_a-u_w)_b$), and B* corresponds to the residual water content (θ_r). As shown in Figure 2, prior to A*, the soil is saturated or nearly saturated, and can be treated as saturated. Beyond B*, there is little water in the soil, so the effects of water content or negative pore-water pressure on soil behavior may be negligible.

What is of great concern in an unsaturated soils is the stage between A* and B*, in which both air and water phases are continuous or partially continuous, and hence the soil properties are strongly related to its water content or negative pore-water pressure. In the formulation of the infiltration process there is a storage term which depends on the matric suction. There will be no overall volume change during the infiltration process.

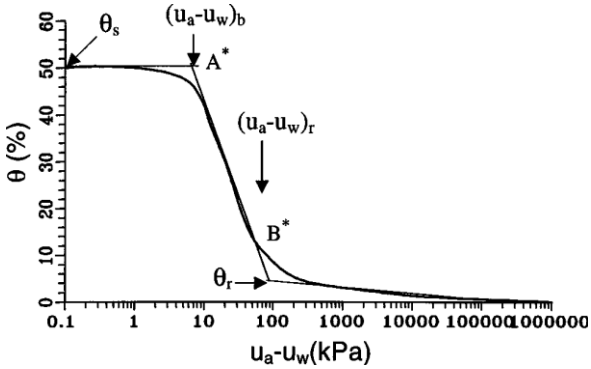

Figure 2 – Soil-Water Characteristic Curve

Water flows only through the pore space filled with water (air-filled pores are not conductive to water). As such, the percentage of the voids filled with water (i.e., degree of saturation) is an important factor.

For an unsaturated soil, the water coefficient of permeability depends on the degree of saturation or negative pore-water pressure of the soil. It can be estimated from the saturated permeability and the characteristics of the SWCC such as; air-entry value, de-saturation rate, saturated, and residual volumetric water contents (Fredlund, and Rahardjo [1], Fredlund et al [2]).

3. Modelling the Infiltration Process

The geometry of a typical cut slope and the boundary conditions utilized for the transient seepage analysis are shown in Figure 3. The sub soil condition in the slope may correspond to Case1, Case 2 or Case 3. In the case of two layered situation the boundary between the two layers is shown by line JC for the thick layer (Case 2) and as line IC for the thin layer (Case 3). Slopes of two different gradients; 1:1 and 1:1.267 were considered in the study.

A boundary flux, q, equal to the desired rainfall intensity, I_r, was applied to the surface of the slope. The nodal flux, Q, was taken to be zero at the sides of the slope above the water table and at the bottom of the slope to simulate a no flow zone (Figure 3). Equal total heads, h_t, were applied at the sides of the slope below the water table.

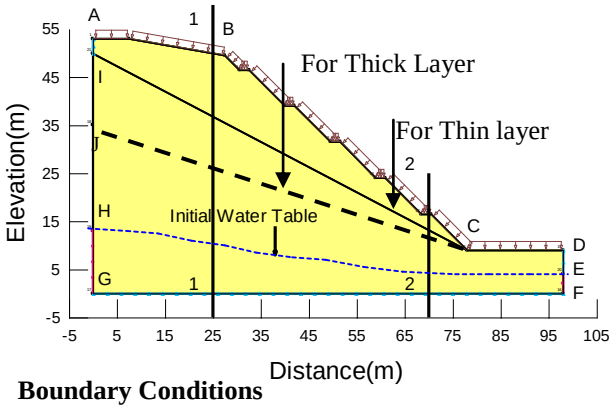

Boundary Conditions

AB, BC, CD = I_r (Rainfall intensity)

AH, DE, FG = Q = 0m^3/s (No flow Boundary)

EF, GH = h_t (Total head at sides)

Figure 3 – Cut Slope Geometry, Selected Sections and Boundary conditions

Residual soil and highly weathered rock were assigned hydraulic conductivity values of 1×10^{-5}m/s and 1×10^{-7}m/s respectively. The saturated volumetric water contents used are 0.45, 0.40 respectively, guided by the published data (Sun et.al- [6]).

The pore water pressure changes in the slopes were computed using a finite element formulation through software SEEP/W [4] taking an initial time step of 0.5 hr, which was varied in an exponential manner as time progressed. In the analysis of this transient flow condition a steady state was assumed within a time step. Using the pore pressure values computed at nodal points, the distributions can be drawn for any section to visualize the effect.

4. Results of Infiltration Studies

4.1 Case 1- Slope Made of Uniform Residual Soil

Kulathilaka and Sujeevan [5], presented the pore water pressure distributions for Section 1-1 and Section 2-2 for rainfall intensities of 5mm/hr and 20mm/hr. (Figure 4 and Figure 5 respectively). For a 5mm/hr rainfall, as rain progressed, the negative pore water pressures near the ground surfaces approached zero at the top level (Section 1-1) and water table has arisen at the lower levels (Section2-2) (Figure 4 (a) and (b)). With a 20mm/hr rainfall, not only the matric suctions were lost but also positive pore water pressures were developed at the top level – a perched water table condition. (Section1-1, Figure 5 (a)). The development of the positive pore water pressure and the rise of the ground water table were more significant at lower levels (Section 2-2, Figure 5 (b)).

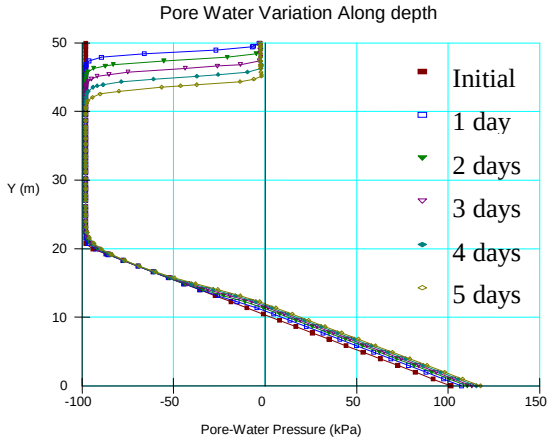

(a) For Section 1-1

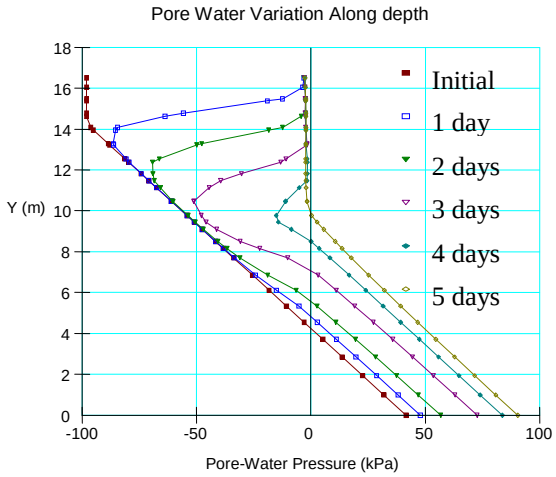

(b) For Section 2-2

Figure 4 –pore water pressure distribution for 5mm/hr rainfall (Case 1)(After Kulathilaka and Sujeevan[5])

Kulathilaka and Sujeevan [5] found that the increase of rainfall beyond 20mm/hr did not result in further increase of pore water pressure. The capacity of infiltration is limited and the extra rainfall contributed to the run off.

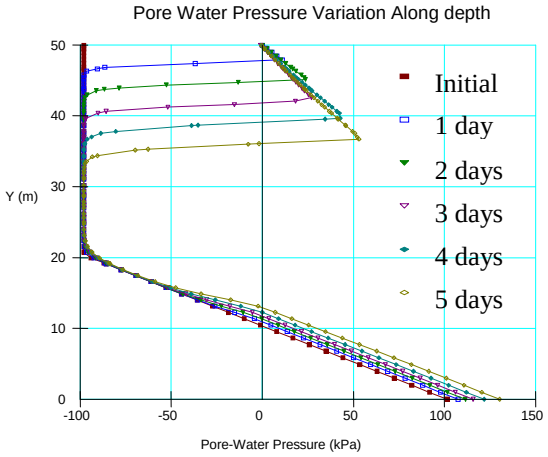

(a) For Section 1-1

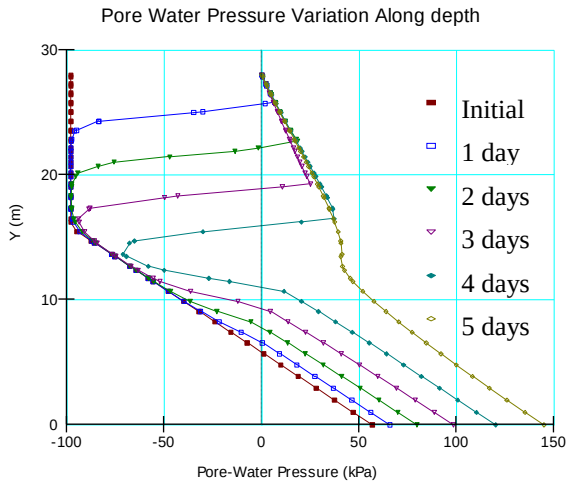

(b) For Section 2-2

Figure 5 –Pore water pressure distribution for 20mm/hr rainfall (Case 1))(After Kulathilaka and Sujeevan [5])

The surface drainage of the cut slope can be enhanced by providing sealed drains over the berms to collect the runoff and cascade drains at appropriate intervals to facilitate the downward movement of the run off in a controlled manner. Further, the slope surface can be provided with a vegetation cover or a fully impermeable artificial cover. Figure 6 presents the protective measures introduced at a location of the STDP at its early stages of implementation. Figure 7 illustrates how the grown vegetation blends with the natural environment and provides the anticipated protection. However, surface protection by vegetation would not be successful under all circumstances. When the soil exposed is highly erodible or made of

weathered and closely fractured rocks methods such as shotcreeting will have to be used. Hong Kong has successfully used Chunam plaster, a mix of soil and cement as an artificial slope cover. With the high variable nature of the slope material, completely different surface protective measures will have to be adopted in close proximity ass illustrated by Figure 8.

With the use of an appropriate vegetation cover on the slope surface infiltration will be reduced due to interception. This will cause an increase of runoff but minimize surface erosion. Evapo-transpiration and root water uptake are two more favourable mechanisms. The system of roots will enhance the cohesion of the soil over a shallow depth. (Wilkinson [8]). A stronger system of roots would provide a soil nailing type effect. An artificial cover such as shotcreeting will completely prevent the infiltration.

Figure 6 – Use of Sealed drains over the berms and cascade drains in the STDP

Figure 7 – Vegetation blends with the natural environment and provides the anticipated protection.

Figure 8 – Different forms of surface protective measures are to be used.

The influence of said surface drainage measures were modeled with the software SEEPW [4] by incorporating a 100mm thick layer of very low permeability 10^{-20}m/s over the berms and a thin layer of low permeability over the slope surface. A parametric study was done by varying the permeability of the thin vegetation layer over the range 10^{-7}m/s to 10^{-9}m/s. Ward [7] has reported permeability values of the order of 10^{-7}m/s in vegetated clay layers. Different techniques such as turfing, hydro seeding etc were successfully used in the STDP. Further field studies should be conducted to identify the most appropriate variety of native vegetation.

A coefficient of permeability in the range 10^{-9}m/s is representative of unfissured clay and would be difficult to achieve with vegetation.

The variation of the pore water pressure distribution for a rainfall of intensity 5 mm/hr when the surface vegetation effect has reduced the permeability to a value of 10^{-7} m/s is presented in Figure 9. The distribution when the permeability of the vegetation layer is reduced to 10^{-9} m/s is presented in Figure 10. These two set of plots should be compared with Figure 4. The response of the pore pressure regime for a rainfall of intensity 20mm/hr with a vegetation cover of permeability 10^{-7}m/s is presented in Figure 11. The case for a cover of permeability 10^{-9}m/s is presented in Figure 12. These figures should be compared with Figure 5.

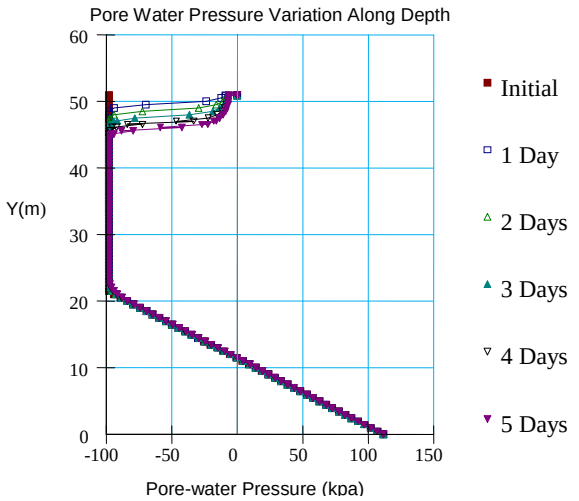

(a) For Section 1-1

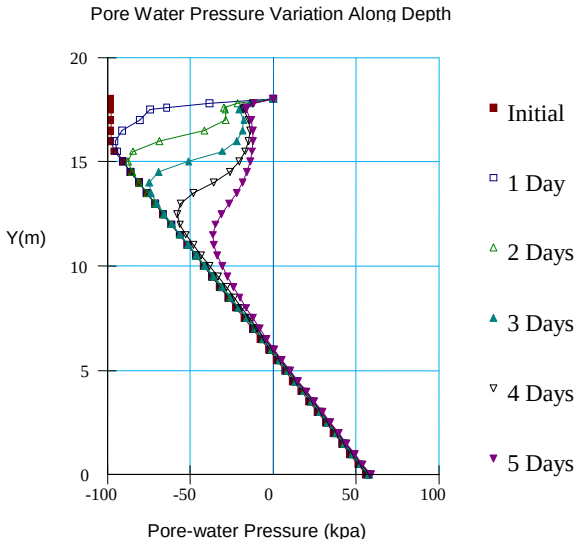

(b) For Section 2-2

Figure 9 –pore water pressure distribution for 5mm/hr rainfall with vegetation layer of permeability 10^{-7}m/s (Case 1)

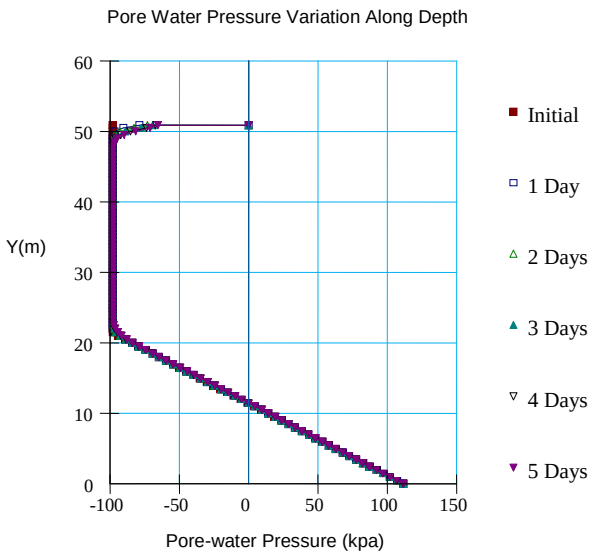

(a) For Section 1-1

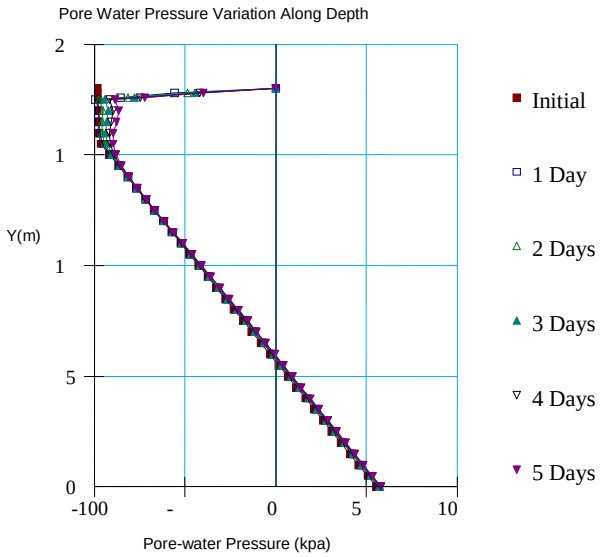

(b) For Section 2-2

Figure 10 – 5mm/hr rainfall with vegetation layer of permeability 10^{-9}m/s (Case 1)

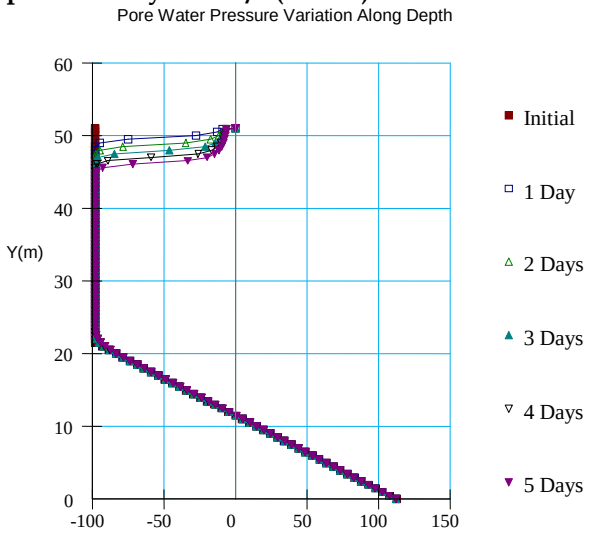

(a) For Section 1-1

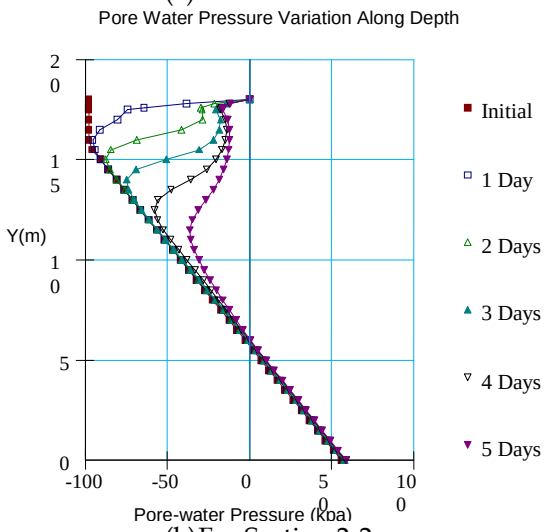

(b) For Section 2-2

Figure 11 – 20mm/hr rainfall with vegetation layer of permeability 10^{-7}m/s (Case 1)

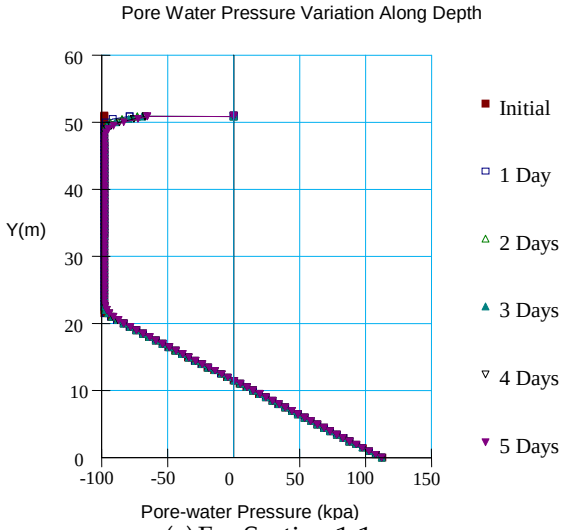

(a) For Section 1-1

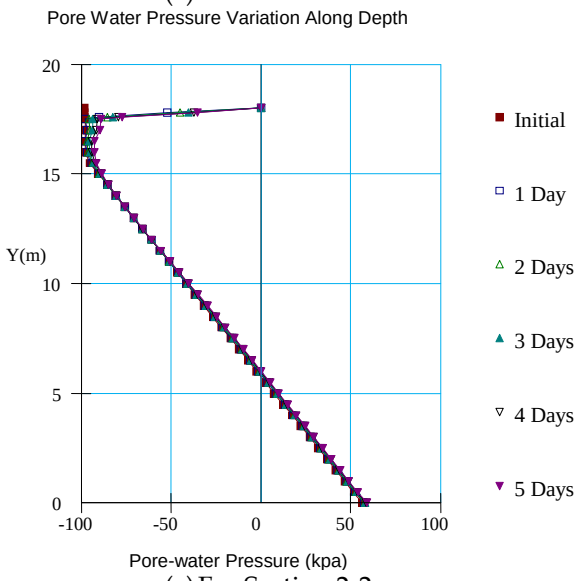

(a) For Section 2-2

Figure 12 – 20mm/hr rainfall with vegetation layer of permeability 10^{-9}m/s (Case 1)

Comparison of Figure 4 and Figure 9 shows that with the vegetation layer of permeability 10^{-7} m/s the complete loss of matric suction was prevented at both section 1-1 and section 2-2. Some matric suction remained even after 5 days of rainfall. The rise of water table at section 2-2 was also prevented.

A similar behavior was witnessed for the rainfall of intensity 20 mm/hr also. The matric suction profiles for section 1-1 and section 2-2 for this rainfall is not very different from that for the 5mm/hr rainfall. With the presence of a vegetation layer of low permeability near the surface, the infiltration of water is restricted and the excess rainfall has contributed to runoff.

It was seen that if the permeability of the vegetation layer was reduced to a value of the order of 10^{-9}m/s, there is virtually no change in the pore pressure regime.(Figure 10 and Figure 12) However, this is difficult to achieve in practice. As such, only the studies with a permeability value of 10^{-7}m/s will be presented in the proceeding sections.

4.2 Case 2- Thick layer of Residual soil over weathered Rock

When a highly weathered rock layer is underlying the residual soil, the downward movement of water is hampered and water gets accumulated at the boundary.

Kulathilaka and Sujeevan [5] presented the pore pressure distributions corresponding to Case 2 for a rainfall of intensity 20 mm/hr (Figure 13). The presence of the less permeable highly weathered rock layer leads to the development of a perched water table at the boundary and increased pore water pressure closer to the surface, in the upper sections of the slopes (Section 1-1 in Figure 13 (a)). Infiltration of water to the lower layer is minimal due to low permeability and water table has not risen as seen in the case of uniform residual soil. (Section 2-2 in Figure 13 (b)).

With the introduction of a vegetation layer of permeability 10^{-7}m/s, the infiltration was significantly reduced and the resulting pore water pressure distribution for rainfall intensity of 20mm/hr is presented in Figure 14. Comparison of Figure 13 and Figure 14 illustrates that the surface vegetation has restricted the infiltration and prevented the development of perched water table near the surface at both section 1-1 and section 2-2. Some matric suction values prevailed even after 5 days of rainfall.

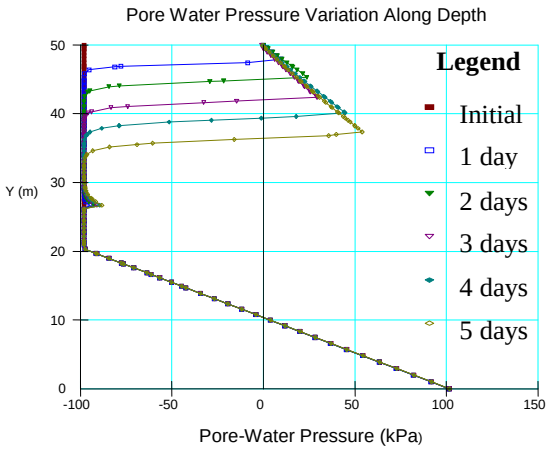

(a) For Section 1-1

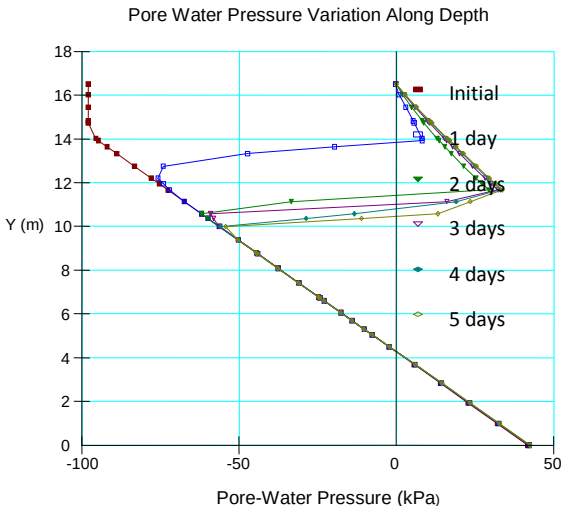

(b) For Section 2-2

Figure 13– Results of 20mm/hr Rainfall - Case 2

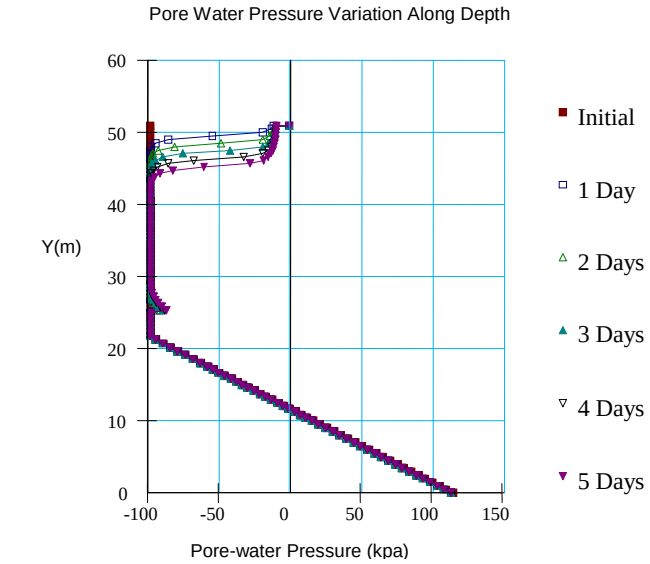

(a) For Section 1-1

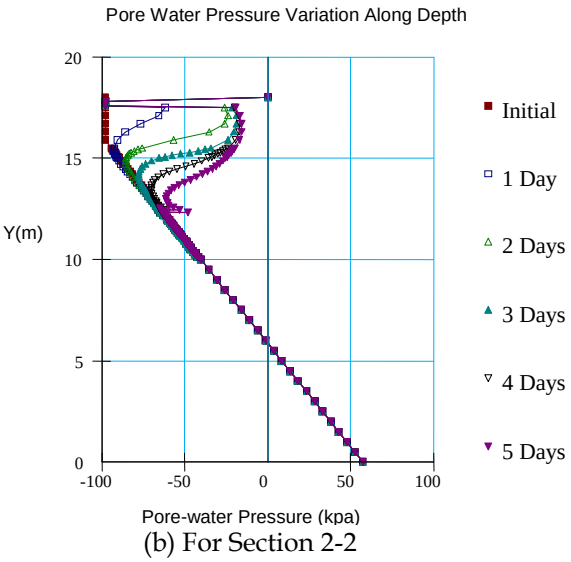

(b) For Section 2-2

Figure 14– Results of 20mm/hr Rainfall with vegetation layer of permeability 10^{-7}m/s - Case2

4.3 Case 3- Thin layer of Residual soil over weathered Rock

Kulathilaka and Sugeevan [5] presented the pore pressure distributions corresponding to case 3 for a rainfall of intensity 20mm/hr (Figure 15). As in Case 2, a perched water table was developed at the boundary and near the surface. The pore water pressure distribution with the introduction of a vegetation layer of permeability 10^{-7}m/s, is presented in Figure 16. Comparisons of Figure 15 and Figure 16 illustrate the effectiveness of the vegetation layer in preventing the development of the perched water table in the layer of thin residual soil. The matic suction loss at section 2-2 is greater even when vegetation is present. This is due to its closeness to the boundary of weathered rock.

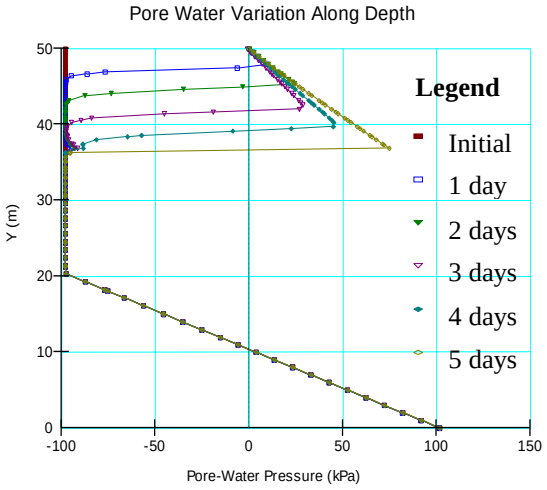

(a) For Section 1-1

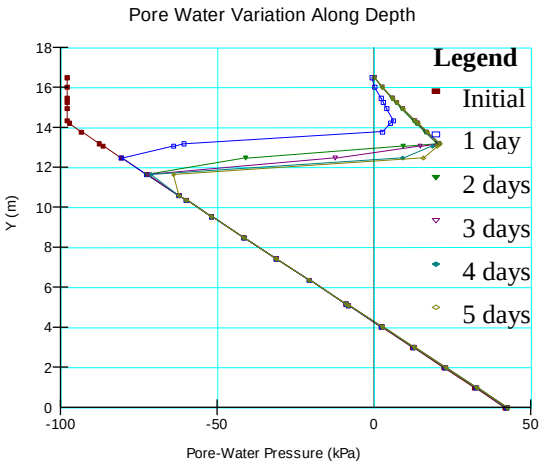

(b) For Section 2-2

Figure 15– Results of 20mm/hr Rainfall for Case3 (After Kulathilaka and Sujeevan 2011)

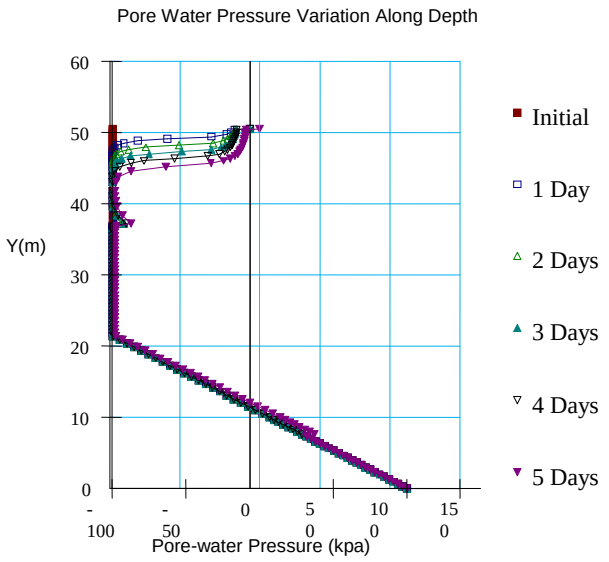

(a) For Section 1-1

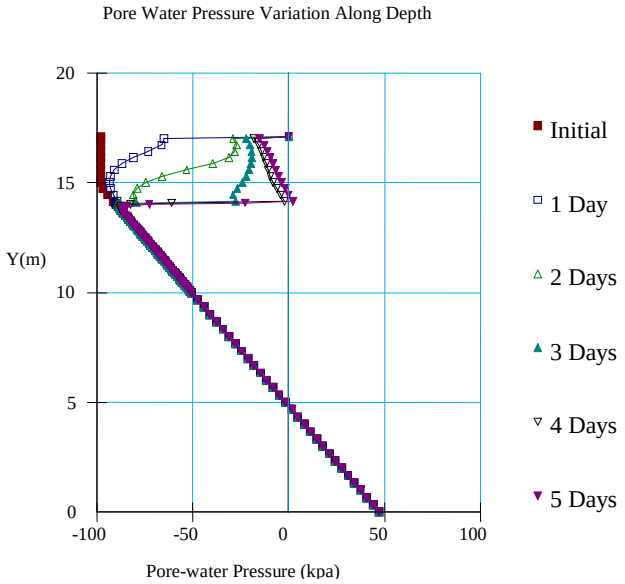

(b) For Section 2-2

Figure 16 – Results of 20mm/hr Rainfall with vegetation layer of permeability 10^{-7}m/s for Case3

4.4 Analysis of Infiltration on the Slope cut to a gradient of 1:1.267

Similar infiltration analyses were done for a slope of gradient 1:1.267, with the three different idealized geological conditions. The observed patterns of variation were similar. With the flatter slope the area available for infiltration was greater and the pore water pressure increase were slightly larger than for the case of slope cut to 1:1 gradient, when the surface drainage measures were not implemented. The detailed results of that analysis is not presented here but will be incorporated in the stability analysis.

5. Slope Stability Analysis

Subsequent to the infiltration study, the stability of the cut slopes under the conditions of Case 1, Case 2 and Case 3, were analyzed incorporating the changes to the pore pressure regime taken place during the period of rainfall. Stability of the slopes were analyzed through the limit equilibrium approach.

Since the loss of matric suction and development of positive pore water pressures is more significant over shallow depths, the potential critical failure surfaces could be non-circular. Circular modes of failure were analyzed by the Bishop's simplified method and non-circular modes of failure were analyzed by the Spencer's method.
The factor of safety (F) is defined as;

$$F = \frac{\tau_f}{\tau_m}$$

Where τ_f =Shear Strength

$$\tau_f = c' + (\sigma_n - u_a)\tan\phi' + (u_a - u_w)\tan\phi^b$$

(Fredlund and Rahardjo 1993).

τ_m =Shear strength mobilized for equilibrium.

The minimum factor of safety (FOS) and the corresponding most critical failure surface at different times into the rainfall event were obtained using the software SLOPE/W [3]. Soil strength parameters used in the slope stability analysis are given in Table 1. Analyses were performed on the two slope geometries; one with cut slope gradient of 1:1 and the other with a cut slope gradient of 1:1.267.

Table 1 – Soil Strength Properties

	Unit Weight (γ_{eff})	Friction angle (ϕ')	(ϕ^b)	(c') kN/m²
Residual Soil	19	34	30	10
HWR	20	40	38	25

6. Results of the Stability Analysis

Kulathilaka and Sujeevan [5] presented the reduction of the safety margins of the 1:1 slope with the rainfall, for the three idealized geological conditions (Figure 17).

Kulathilaka and Sujeevan [5] also presented the variation of the factor of safety of the slope cut to a gradient 1:1.267 (Figure 18). The comparison showed that even though the slope cut to a gradient of 1:1.267 had a greater safety margin during the dry weather, it reduced to the same values as the slope cut to a 1:1

gradient, after 2-3 days of rain. As such, it is clear that if proper drainage measures are not adopted, making the slope flatter alone would not guarantee safety under the conditions of prolonged rainfall. Surface drainage can be enhanced by providing sealed berm drains, cascade drains and slope surface coverage.

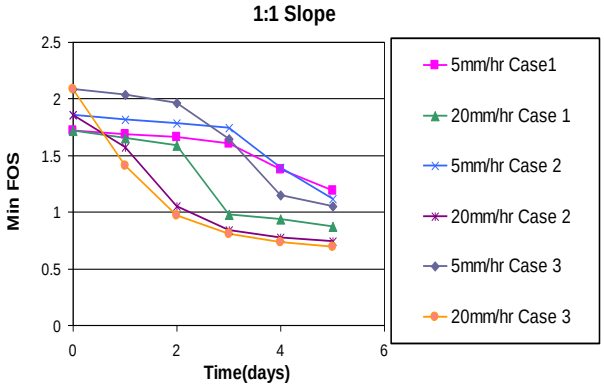

Figure 17: Variation of factor of safety with duration of rainfall - 1:1 slope (After Kulathilaka and Sujeevan [5])

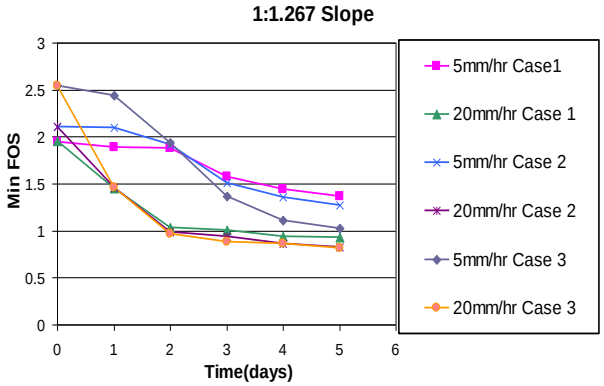

Figure 18: Variation of factor of safety with duration of rainfall –1:1.267

The effectiveness of the berm drains and vegetation cover in maintenance of a sufficient safety margin in the slope even with a prolonged rainfall is illustrated through Figure 19. For the Case1 (uniform slope) cut to a 1:1 gradient, the variation of factor of safety under conditions of; slope with sealed berm drains only, slope with vegetation cover of permeability 10^{-7} m/s are compared in Figure 19. It could be seen that the vegetation cover which reduced the infiltration and loss of maric suction had been effective in maintaining a significant margin of safety during the prolonged rainfall. When there is no protective vegetation cover, the factor of safety reduced significantly as the rain persists. When the vegetation cover is present the reduction of the factor of safety with the prolonged rainfall is very minimal. The difference of the factor of safety values corresponding to rainfall intensities of 5 mm/hr and 20 mm/hr is negligible. The surface vegetation layer of low permeability has restricted the infiltration and major part of the rainfall has ended as runoff.

The behaviour of the slope under Case 2 and Case 3 presented in Figure 20 and Figure 21 respectively, confirms the effectiveness of the vegetation layer.

This importance of achieving a sufficiently low permeability in the vegetation layer is highlighted by Figure 22 where the behavior of the slope with a vegetation layer of permeability 10^{-6}m/s is presented. It is seen that there is a significant reduction of the factor of safety as the rainfall prolongs.

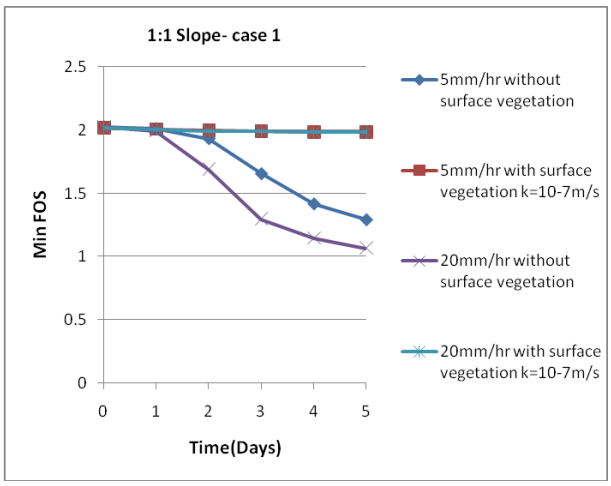

Figure 19 –Variation of factor of safety with duration of rainfall - 1:1 slope- Case 1

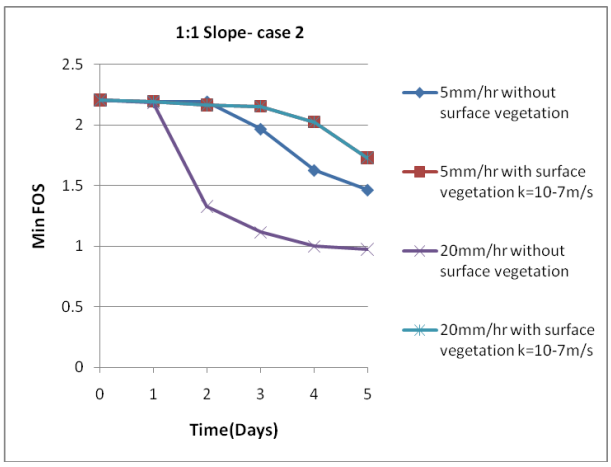

Figure 20 –Variation of factor of safety with duration of rainfall - 1:1 slope- Case 2

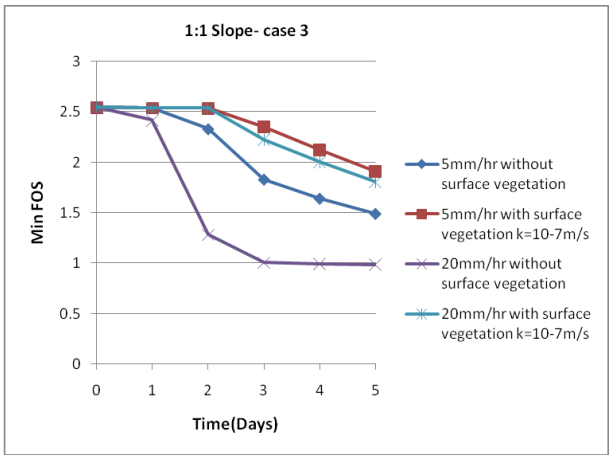

Figure 21 –Variation of factor of safety with duration of rainfall - 1:1 slope- Case 3

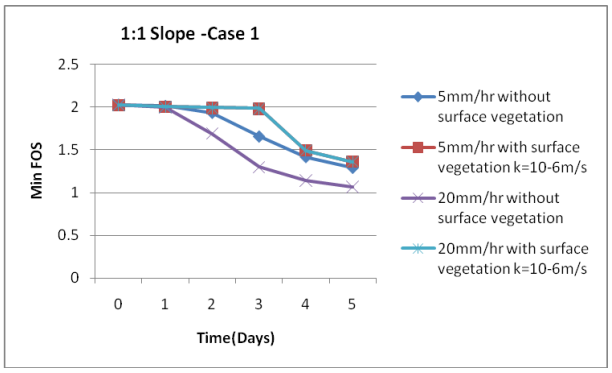

Figure 22–Factor of safety with duration of rainfall – Vegetation of permeability 10^{-6}m/s- 1:1 slope- Case 1

The effectiveness of the vegetation cover and the other measures of surface drainage, on the stability of the slope cut to 1:1.267 gradient is presented in Figure 23, for Case 1. The behavior of Case 2 and Case 3 are similar to that of the slope cut to 1:1 gradient respectively.

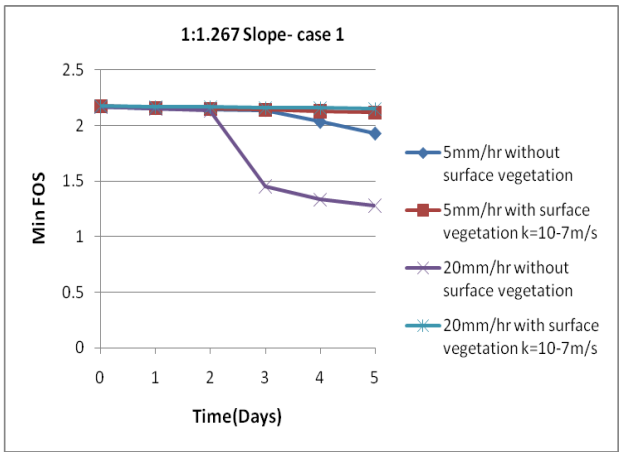

Figure 23 –Variation of factor of safety with duration of rainfall - 1:1.267 slope- Case 1

The loss of matric suction, with the rainfall initiates near the surface and the greatest effect on the reduction of shear strength is closer to the ground surface. As such, the critical failure surfaces corresponding to the latter stages are much shallow as illustrated by Figure 24. With the vegetation cover in place, the matric suction reduction was minimal and critical failure surfaces are somewhat deeper as presented in Figure 25.

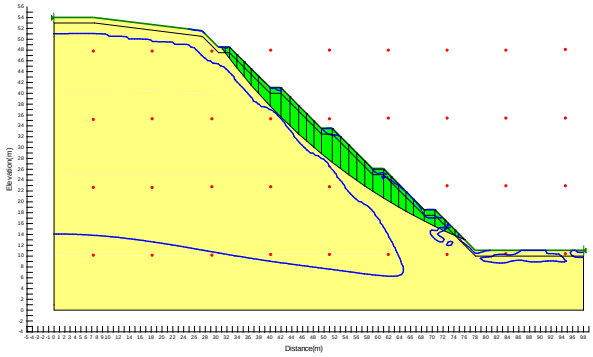

Figure 24: Shape of a typical failure surface without vegetation cover – Case1

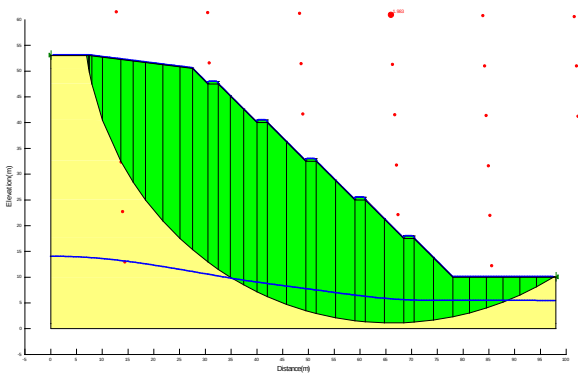

Figure 25: Shape of a typical failure surface with vegetation cover 10^{-7}m/s – Case 1

7. Other Methods of Stabilization

If the water table rise estimated from the infiltration analysis appears to be too high sub surface drains may have to be used. Perforated drains installed in holes bored at an upward angle around 10°, at appropriate spacings will facilitate the rapid dissipation of ore water pressures developed. In some other instances further methods of strengthening such as soil nailing will have to be used.

8. Maintenance of Stabilization Measures

It is essential to closely monitor the surface and sub surface drainage and surface protection measures installed to ensure that they are able to perform the designed function. A minor defect left unattended

may lead to a catastrophic failure. A systematic process of observation and identification of defects, especially prior to anticipated periods of heavy rainfall should be established. Critical repair work needed should be promptly attended.

7. Conclusions

Failures in slopes made of residual soils are often triggered by rainfall. As such, it is very important to understand the mechanisms involved and procedures that can be adopted to negate the effect of rainfall.

The reduction of the matric suctions in a slope made of unsaturated residual soils due to prolong rainfalls of different intensity and the effectiveness of a thin vegetation cover of reduced permeability in minimizing the effect of prolonged rainfall was studied.

The results showed that the use of a 100 mm thick vegetation cover of permeability 10^{-7}m/s, which is practically achievable, could cause a significant reduction in infiltration and prevent the formation of a perched water table and minimize the destruction of the matric suction. The study was done for different geological condition of a uniform residual soil and a residual soil underlain by weathered rock,(Case1, Case 2 and Case3) and all three geological conditions showed a similar response.

The study also revealed that if the vegetation cover is more permeable with a permeability of the order of 10^{-6} m/s it would be less effective in maintaining a sufficient safety factor during a prolong rainfall. As such, Studies should be conducted to identify appropriate type of vegetation.

The study revealed that the use of a berm drains alone is not sufficient. The berm drains and cascade drains along with a vegetation cover of practically achievable reduced permeability will minimize the changes in the pore pressure regime and help to maintain sufficient safety margins during the periods of heavy rainfall. In some instances additional safety measures such as sub surface drains and soil nailing may be required.

Systematic monitoring and maintenance of these stabilization measures is extremely important to ensure that they perform their designed functions.

8. References

1. Fredlund, D. G., and Rahardjo, H. (1993). "Soil Mechanics for Unsaturated soils", Wiley, New York.
2. Fredlund, D. G., Xing, A. and Huang, S. Y. (1994)." Predicting the Permeability Function for Unsaturated Soils Using the Soil-Water Characteristic Curve, Canadian Geotechnical Journal Vol 31, pp 533-546.
3. GEO-SLOPE International Ltd. (2007)-a . "Stability Modeling with SLOPE/W 2007- An Engineering Methodology" Calgary, Alberta, Canada, Second Edition, May 2007.
4. GEO-SLOPE International Ltd. (2007)-b "Seepage Modeling with SEEP/W 2007-An Engineering Methodology" Calgary, Alberta, Canada, Second Edition, May 2007
5. Kulathilaka S A S and Sujeevan V (2011), Effects of Rainfall on Stability of Cut Slopes in Residual Soils , A paper published in the 14 th Asian Regional Conference in Soil Mechanics and Geotechnical Engineering to e held in Hong Kong in May 2011
6. Sun.H.W, Wong. H.N and Ho. K.K.S (1998) "Analysis of infiltration in unsaturated ground", *Slope Engineering in Hong Kong, Li, Kay & Ho(eds)*© 1998 Balkema, Rotterdam, ISBN 90 5410935 1.
7. Ward A. L. (2007) – Geotechnical, Hydrologic and Vegetation package for 200-UW-1_ Waste Site Engineered Surface Barrier Design, Report submitted to US Department of Energy.
8. Wilkinson P. L. (2000), Investigating the Hydrological Effects of Vegetation on Slope Stability: Development of a Fully Integrated Numerical Model, PhD Thesis at the Department of Geotechnical Services, University of Bristol.

BEHAVIOUR OF STIFFENED DEEP MIXING CEMENT PILES IN BANGKOK CLAY

D. T. Bergado[a], P. Jamsawang[b], J.S.M. Fowze[b], T. Suksawat[c], P. Voottipruex[d], and W. Cheng[e]

[a] Professor in Geotechnical Engineering Program, School of Engineering and Technology, Asian Institute of Technology , Thailand (GTE-AIT)
[b] Doctoral Graduate, GTE-AIT
[c] M. Eng. Graduate, GTE-AIT
[d] Assoc. Professor in Faculty of Technical Education, King Mongkut's University of Technology North Bangkok, Thailand.
[e] Regional Technical Manager of PLAXIS Asia.

ABSTRACT

The characteristics of soft clay are low strength, high compressibility and low permeability. Many methods have been used to improve the soft clay ground. These methods include in-situ earth reinforcement and piles of various materials, including partial or complete ground replacement, geotextiles, preloading, grouting, deep mixing pile or sand pile; timber or concrete piles: micro piles, cast-in-situ piles. These improvement methods all have their advantages and disadvantages.

Deep mixing (DM) techniques, developed during 1960's, were first reported in the literature in the early 1970's and has widely been used to improve the engineering properties of thick deposits of soft ground. Although, deep cement mixing (DCM) piles can effectively reduce settlements of full-scale embankments, they are characterized by variable strength and stiffness, specifically, flexural strength leading to low bearing capacity and large settlements. Furthermore, DCM piles can also be subjected to horizontal forces induced by the embankment loads to which they have low resistance.

DCM piles, thus, stiffened (SDCM) by employing a precast concrete pile inserted at their centers were studied for their behavior under field full scale pile and embankment loads, and using numerical simulations. Results confirm the superiority of the new technology over the traditional technology of DCM piles

Keywords: soft bangkok clay, embankment loading, deep cement mixing (DCM), stiffened deep cement mixing (SDCM), soft soil improvement

INTRODUCTION

Deep cement mixing (DCM) pile is widely used to support embankments and lightly-loaded structures on soft ground. The behavior of the DCM pile under embankment loading on soft Bangkok clay has been studied by Chen (1990), Honjo et al. (1991), Bergado et al. (1999), Lin and Wong (1999) and Lai et al. (2006). DCM piles have been shown to have variable strength and stiffness due to poor workmanship (Petchgate et al., 2003a, b; 2004) leading to low bearing capacity and large settlements for piles failure instead of soil failure (Fig. 1(a)). Fig. 1(b) shows the loading test results of DCM piles in soft Bangkok clay by Petchgate (2003a, b). The results of the field tests show almost half of the DCM piles failed by pile failure instead of soil failure. In the case of pile failure, the bearing capacity of the DCM pile tends to be lower than the design load of 10 tons (below the black line in Fig. 1(b)) implying low quality DCM material.

Another problem is that DCM piles are sometimes subjected to both vertical and horizontal forces induced by the embankment loads even though they are not suitable for medium to high design loads (Dong et al., 2004). If DCM piles are to be subjected to a heavy load, the designer needs to ensure a higher ground improvement ratio, which can be achieved by a larger amount of cement and higher strength cement. Therefore, a new technology called the Stiffened Deep Cement Mixing (SDCM) pile employs a precast concrete core pile inserted at the center of DCM pile. This concrete core pile takes most of the load and transmits it to the surrounding soil-cement through the interfaces between the concrete core pile and the DCM pile. The SDCM pile is more suitable than the DCM pile because the SDCM pile has higher strength and stiffness and can sustain both higher bending moments and higher lateral loads. A series of pile load tests were conducted to investigate the behavior of SDCM piles in China by Dong et al. (2004), Wu et al. (2005), and Zheng et al. (2005). Most of the tests were only concerned with the bearing capacities of the SDCM piles. Recently, Jamsawang et al. (2008) measured and simulated the settlement behavior of composite foundations consisting of a SDCM pile with a concrete core pile in laboratory model tests.

In this paper, comprehensive research results on the behavior of Stiffened Deep Cement Mixing (SDCM) are presented and compared to the behavior of the traditional Deep Cement Mixing (DCM). Included are the test results and analyses of field full scale load tests on DCM and SDCM piles as well as their behavior under a 5 m high full scale embankment loading. The results of the 3D numerical simulations performed in order to back analyze the design parameters are also reported, and these parameters were utilized further in numerical experiments which considered sensitivity and also in calibrated FEM analyses.

Stiffened Deep Cement Mixed (SDCM) Piles

Stiffened deep cement mixing (SDCM) pile is a composite structure of concrete core pile and deep cement mixing pile. The prestressed concrete core pile is inserted into the center of the DCM pile immediately after the construction of wet mixing DCM pile. The two parts of the composite piles work together by supporting and transferring the vertical load effectively to the DCM pile and to the surrounding soil. In the SDCM pile, the DCM pile forms the surrounding outer layer supporting the concrete core pile, in effect of increasing its stiffness and ability to resist the compressive stresses along the pile shaft. It should be noted that this novel method of improving the strength of DCM pile has been referred to by different terminology over the years, including the concrete cored DCM pile (Dong et al., 2004), the composite DMM column (Zheng et al., 2005) and the stiffened deep cement mixed (SDCM) column method (Wu et al., 2005). Each SDCM pile was constructed by inserting a prestressed concrete core pile in the middle of a DCM pile with a 0.6 m diameter and length of 7.0 m (Fig. 2(a)). The jet grouting technique, using a jet pressure of 22 MPa with a water-cement ratio of 1.5, was utilized in the installation of the DCM piles. The concrete core pile was inserted into the SDCM pile immediately after the deep mixing process had completed. During the curing period, the concrete core pile was anchored at the ground surface to prevent it from sinking. The deep mixing piles were allowed to cure for about 80 days. The prestressed concrete pile was selected as the stiff core because of its high strength and stiffness and also because it is cheaper than steel pile. The concrete core pile (Fig. 2(b)) consisted of 0.18×0.18 m and 0.22×0.22 m square cross sections and 4.0 and 6.0 m in lengths corresponding area ratio, defined as the sectional area of core pile over a sectional area of the DCM pile (A_{core}/A_{DCM}), and length ratio, defined as the length of core pile over the length of the DCM pile (L_{core}/L_{DCM}), of 0.11 and 0.17 as well as 0.57 and 0.85, respectively (Table 1).

The compressive strength of the concrete core pile was found to be 35 MPa. For the numerical simulation, the length of the concrete pile was varied from 1.00 m to 7.00 m with 1.0 m increments to evaluate the effect of the length of the concrete core pile on the capacity of the SDCM pile. The Mohr-Coulomb model was recommended to simulate the concrete core pile instead of the linear elastic model because its stiffness can be overestimated if the tensile strain is large enough to crack the concrete (Tand and Vipulandan, 2008).

Project Site and Subsoil Profile

Full scale axial and lateral pile load tests were performed by Shinwuttiwong (2007) and Jamsawang (2009) within the campus of Asian Institute of Technology (AIT). The site is situated in the central plains of Thailand famous for its thick layer deposit of soft Bangkok clay. The foundation soils and their properties at the site are shown in Fig. 3. The uppermost 2.0 m thick layer is weathered crust, which is underlain by 6.0 m of a thick soft to medium stiff clay layer. A stiff clay layer is found at the depth of 8.0 m from the surface. The undrained shear strength of the soft clay obtained the from field vane test was 20 kPa and the strength of the stiff clay layer below the depth of 8.0 m from the surface is more than 40 kPa (Bergado et al., 2002b). The other parameters are shown in Table 2.

FULL SCALE PILE LOAD TESTS

Testing Program

A series of full scale load tests on SDCM and DCM piles under axial compression load and lateral load were performed to determine their ultimate bearing capacities and lateral resistances. In addition, two pullout interface tests between the concrete core and deep cement mixing were also conducted to determine the interface resistance between the concrete core and the deep cement mixing pile. The full scale test was monitored in order to study its consolidation and deformation behavior and the performances of the SDCM and DCM pile foundations were compared. The SDCM and DCM piles were constructed beneath the test embankment with 2.0 m spacing (Fig. 4).

Unconfined Compression Tests on Deep Cement Mixing Core Samples

To obtain the engineering properties of the DCM pile in the test site, three DCM piles were constructed (Fig. 4) so that core samples could be extracted for unconfined compression tests in the laboratory in order to determine the unconfined compressive strength, q_u, and the modulus of elasticity corresponding to 50% unconfined compressive strength, E_{50}. Unconfined compressive tests were performed on samples 50 mm in diameter and with a height of 100 mm. The values were scattered over the entire depth without any clear trend of the influence of the depth on the values of unconfined compressive strength and the modulus of elasticity (Fig. 5(a)). The values of unconfined compressive strength ranged from 500 kPa to 1,500 kPa with an average value of 900 kPa while the modulus of elasticity ranged from 50,000 kPa to 150,000 kPa with an average value of 90,000 kPa, indicating that $E_{50} = 101 q_u$ as is shown in Fig. 5(b). It can be seen that the correlation ratio of $E50/q_u$ obtained from field coring samples ranged from 60 to 150.

Axial Load Tests

Two axial load tests on SDCM piles (SDCM-C1 and SDCM-C2) and two axial load tests on DCM piles (DCMC1 and DCM-C2) were conducted in accordance with ASTM D-1143, Quick Load Test

Method for Individual Piles under Static Axial Compression Load. The load was applied in increments of 10 kN. Each load increment was maintained for 5 min. The load was applied until continuous settlement occurred with either a slight increase or no increase in the axial load. Figure 6 shows the axial compression load versus the settlement relationships for all four test piles. The ultimate bearing capacities of all test piles were determined by the slope tangent method at the point of intersection of the initial and final tangents in the load settlement curve, as established by Butler and Hoy (1977). The ultimate bearing capacities of the DCM piles, DCM-C1 and DCM-C2, were 220 kN and 140 kN, respectively. The large difference in the ultimate bearing capacities of DCM-C1 and DCM-C2, as much as 80 kN, confirmed the low quality that commonly occurs in DCM piles which results in its low bearing capacity (Petchgateet al., 2003a). The ultimate bearing capacities of the SDCM piles, SDCM-C1 and SDCM-C2, were 320 kN and 310 kN, respectively. No significant difference in the ultimate bearing capacities of these SDCM piles and their load settlement curves was observed. Their more consistent ultimate bearing capacities imply that the concrete core improved the quality and increased the bearing capacity as well as the stiffness of the SDCM pile. The average ultimate bearing capacity of the SDCM pile with a 0.22 m square and 6 m long concrete core pile was 315 kN, which is 1.4 and 2.2 times, respectively, higher than those of DCM-C1 and DCM-C2 piles.

Lateral Load Tests

Two lateral load tests on SDCM piles (SDCM-L1 and SDCM-L2) and two lateral load tests on DCM piles (DCM-L1 and DCM-L2) were conducted in accordance with ASTM D-3966, Standard Lateral Loading Procedure. The load was applied in increments of 1 kN. Each load increment was maintained for 10 min. The load was applied until continuous lateral displacements occurred with either a slight increase or no increase in load. Figure 7 shows the lateral load versus the lateral displacement relationships for all four test piles. The ultimate lateral loads of the DCM piles, DCM-L1 and DCM-L2,were 3.5 kN and 2.5 kN, respectively, with an average ultimate lateral load of 3.0 kN, which is very low due to the low flexural strength (Terashi and Tanaka, 1981; Petchgate et al., 2004). The ultimate lateral loads for the SDCM piles, SDCM-L1 and SDCM-L2, were 46 kN and 45 kN, respectively, with an average ultimate lateral load of 45.5 kN, which is 15 times greater than that for the DCM pile. Moreover, much less lateral displacement was observed for the SDCM pile than for the DCM pile at the same load, implying that the SDCM pile has much higher flexural stiffness than the DCM pile. Based on the compression and lateral load tests, SDCM piles, with their higher stiffness and ultimate bearing capacity, and especially higher flexural stiffness and strength, are more suitable than DCM piles for embankment foundations subjected to vertical and horizontal loads.

Pullout Load Tests

Finally, two pullout load tests (Pullout-T1 and Pullout- T2) were performed in accordance with ASTM D-3689, Quick Load Test Method for Individual Piles under Static Axial Tensile Load. The length of the concrete core pile embedded in SDCM pile was 1.0 m for all tests. The load was applied in increments of 5 kN. Each load increment was maintained for 5 min. The load was applied until continuous vertical displacements occurred with a slight increase or no increase in load. Figure 8 shows the tension load versus vertical displacement relationships. The maximum tension loads were 165 kN and 155 kN for the test piles, Pullout-T1 and Pullout-T2, respectively, with average maximum tensile load of 160 kN. The interface shear strength ($\tau_{interface}$) was calculated by dividing the maximum tensile load by the surface area of the concrete core embedded in the DCM pile.

Consequently, the strength reduction factor for interfaces (Rinter) defined by Brinkgreve and Broere (2006) is:

$$R_{inter} = \tau_{interface}/c_{soil} = 182/450 = 0.40 \quad (1)$$

This value is within the range of pullout interface test results on concrete core and cement-admixed clay performed in the laboratory by Jamsawang et al. (2008), ranging from 0.38 to 0.46.

TEST EMBANKMENT ON SOFT GROUND IMPROVED WITH DCM AND SDCM PILE

Installation of Foundation Improvement

Prior to embankment construction, the foundation subsoil was improved with SDCM and DCM piles. The DCM piles were installed in situ by a jet mixing method employing a jet pressure of 22 MPa. Both SDCM and DCM piles were installed at 2.0 m spacing as shown in Figs. 9(a) and (b). The water-cement ratio (w/c) of the cement slurry and the cement content employed for the construction of deep mixing were 1.5 and 150 kg/m^3 of soil, respectively. Each deep mixing pile had a diameter of 0.6 m and a length of 7.0 m and penetrated down to the bottom of the soft clay layer, as shown in the section view of the embankment (Fig. 9(b)).

Field Instrumentations

To observe the behavior of SDCM and DCM piles under embankment loading as well as the behavior of the test embankment, various instruments were installed at the site. Figures 9(a) and (b) show the instrumentation in plan and cross-sectional views, respectively. Five surface settlement plates were installed to a depth of 1.0 m from the original ground. The surface settlement plates were installed on both the top of the SDCM pile (S10) and DCM pile (S11), on the surrounding clay of SDCM pile (S1) and DCM pile (S7) and on the unimproved clay (S4). The installations were carried out after an excavation of 1.0 m depth, the base level of the test embankment. Six subsurface settlement gauges were also installed at 4.0 m and 7.0 m depths from the original ground. Subsurface settlement gauges were installed in the surrounding clay of the SDCM pile (S2 and S3), the DCM pile (S7 and S8) and in the unimproved clay (S5 and S6). Three piezometers were installed at 4.0 m depths from the original ground in the surrounding clay of SDCM pile (P1) and DCM pile (P3) and in the unimproved clay (P2). Four vertical inclinometer casings were installed. The vertical inclinometer casings were installed in the SDCM pile (I1), the DCM pile (I3), the surrounding clay of the SDCMpile (I2) and the surrounding clay of the DCM pile (I4).

Construction of Embankment

A 5 m high test embankment was constructed at the northern part of the Asian Institute of Technology (AIT) Campus, Thailand. The undrained shear strength of the uppermost 2 m thick weathered crust layer is significantly higher than that of the soft clay layer below. In order to obtain better deformation characteristics of the improved ground for both SDCM and DCM piles, a 1 m depth of weathered crust was excavated. Accordingly, prior to the embankment construction, a 21 m wide, 40 m long and 1 m depth foundation soil was removed. After the excavation of the trench, the area covered by the test embankment was backfilled with 1.0 m depth compacted silty sand. The silty sand was compacted to a unit weight of 17 kN/m3 by a vibratory roller. The area around the instruments was compacted by a vibratory hand compactor. Then, a 5 m high embankment was

constructed with end slopes of 1:1 and side slopes of 1:1.5 with base dimensions of 21 m by 21 m and top dimensions of 9 m by 6 m (Figs. 9(a), (b)). The embankment material mostly consisted of weathered clay excavated from the area near the test embankment. The weathered clay was compacted to 0.30 m lift thickness to a density of 16 kN/m^3. The embankment construction was completed within 30 days.

FIELD EMBANKMENT TEST RESULTS

Settlement Behavior of SDCM Pile and DCM Pile Improved Soft Clay Foundation

Figure 10 shows the settlements on top of the SDCM pile, the DCM pile, the surrounding clay of the SDCM pile, the surrounding clay of the DCM pile and on the surface of the unimproved clay during and after construction, and up to 570 days of full embankment loading. Approximately 50z of the total settlement occurred during the 30 days of construction of the test embankment. The settlement on the surrounding clay of the SDCM pile was slightly less than that on the surrounding clay the DCM pile. Thus, the embankment load was transferred to the SDCM pile more efficiently than to the DCM pile. Moreover, the settlement on the SDCM pile is 40z less than the corresponding value on the DCM pile due to its higher stiffness. In addition, the settlements on top of the SDCM piles were almost 60z less than that of the unimproved ground.

Lateral Movements of SDCM and DCM Piles

The lateral movements of SDCM and DCM piles were obtained from inclinometers I1 and I3, respectively. The locations of the inclinometers are shown in Fig. 9(b). The comparison of the lateral movement profiles of the SDCM and DCM piles is shown in Fig. 11(a). About 65z and 55z of the total lateral movements occurred immediately after the construction of the test embankment for SDCM and DCM piles, respectively. Due to its higher flexural stiffness, the lateral movement in the SDCM piles was 60z that of the DCM pile.

The lateral movements of the surrounding clay adjacent to SDCM and DCM piles (Fig. 11(b)) were obtained from inclinometers I2 and I4, respectively, whose locations are indicated in Fig. 9(b). The measured maximum lateral movements at a depth of 1.0 m (excavation base level) immediately after embankment construction and after 570 days for the surrounding clay of the SDCM pile amounted to 18.3 mm and 28.3 mm, respectively, while those for the surrounding clay of the DCM pile amounted to 36.0 mm and 67.3 mm, respectively. Thus, about 65z and 50z of the total lateral movement occurred during the construction of the test embankment for the adjacent clays of the SDCM piles and the DCM piles, respectively. This indicates that the SDCM pile was capable of reducing the magnitude of lateral movement by 60%. Therefore, the SDCM and DCM piles were confirmed to move laterally together with their adjacent ground.

THREE-DIMENSIONAL FINITE ELEMENT SIMULATION

Finite Element Discretization

Finite element simulations were performed using the 3D FEM simulations developed by Brinkgreve and Broere (2006) since these allow for a realistic simulation of the construction sequences. The basic soil elements were represented by the 3D, 15-node wedge elements (6-node triangles in horizontal direction and 8-node quadrilaterals in a vertical direction). The axial compression and

lateral simulation ware consisted of an SDCM pile, a DCM pile and sub-soil foundations, as shown in Figs. 12(a) and (b). In Fig. 12(a), the finite element mesh, composed of more than 3,750 elements, is given, and in Fig. 12(b), the SDCM pile at the center of the model is shown. For the boundary condition, the bottom of model is fixed in all directions the surface is free in all directions. The vertical model boundary with their normal direction is fixed and the other directions are free (i.e., vertical model boundary in x-direction such as parallel to the y-z plan is fixed in the x-direction and free in the y and z directions). The DCM pile was modeled as volume elements capable of simulating the deformation and stresses. The prestressed concrete core pile inserted at the center of SDCM pile was modeled as a ``massive pile", and was composed of volume elements. Interface elements modeled with 16-node interface elements were assigned around the periphery of the concrete core. The interface elements consisted of eight pairs of nodes, each of which was compatible with the 8-noded quadrilateral side of the soil element. The distance between the two nodes of a node pair was zero. Each node had three translational degrees of freedom. Consequently, the interface elements allowed for differential displacement between the node pairs (slipping and gapping). Interface elements are required to have the strength reduction factors, R_{inter}, which are the fraction of the surrounding soil strengths (cohesion and/or friction) effectively mobilized at the interface.

Material Models and Parameters

Although the prestressed concrete core pile has much higher strength and stiffness than the DCM pile, by 40 and 300 times, respectively, failure took place not only within the DCM material (pile failure) but also in the concrete core piles (pile failure) especially during the lateral load tests. Consequently, the Mohr-Coulomb model (MCM) was used to simulate the prestressed core pile by referring to all the parameters from the compression test as well as the simulation in the PLAXIS 2D V8.5. The interface strength reduction factor of 0.4 obtained from the full scale pullout load test discussed earlier was used for the interface behavior between the core pile and the DCM material. The Mohr-Coulomb model (MCM) was selected to model the behavior of the DCM piles. The vertical permeability of the DCM pile of 30 times that of the surrounding soil was based on the back-analysis using 2D PLAXIS software conducted by Lai et al. (2006). The backfill soil materials used in the embankment were compacted silty sand and weathered clay. The MCM was used to represent the compacted embankment materials, as tabulated in Table 2. The effective cohesion, friction angle and deformation characteristics of the backfill materials were determined from consolidated undrained triaxial (CIU) tests using representative specimens as well as the densities of the embankment materials. The MCM was used to model the weathered crust layer, medium stiff clay layer and stiff clay layer. The material properties were obtained from the previous test data on Bangkok clay (Balasubramaniam et al., 1978). The soft clay layer from 2 m to 8 m depth was modeled by the Soft Soil Model (SSM). The SSM is a Cam-clay type model developed by Vermeer and Brinkgreve, 1995. The material properties were obtained from the previous test data on Bangkok clay (Balasubramaniam et al., 1978) and the result of previous investigations (Chai 1992; Bergado et al., 1995; Bergado et al., 2002a, b). The FEM parameters for all the materials are also tabulated in Table 2.

Simulated versus Observed Data

Figure 13 shows the results of the simulations compared to the observed data when the cohesion of the DCM pile, c'_{DCM}, was varied from 100 to 300 kPa. The cohesion of the DCM pile significantly affected the ultimate bearing capacity of the DCM pile but the corresponding small effect on the

SDCM pile implied that the core pile supported most of the load and transferred smaller proportions of the load to the tip of the core pile. For the axial compression of both DCM and SDCM piles, the effective cohesion, c'_{DCM} of 200 kPa is the best fit to the measured data.

Using a 3D FEM simulation, the sensitivity analysis of the load-settlement curves of the SDCM pile was performed by varying the interface strength reduction factor, R_{inter}. The shapes of the curves were affected by the R_{inter} values, as shown in Fig. 14. The R_{inter} values from 0.40 to 1.0 yielded slightly different load-settlement curves. However, the R_{inter} on 0.40 yielded good agreement between the observed and simulated data, thus confirming the results of the pullout-test. Figure 15(a) shows the results of the simulation of the effect of the tensile strength of the DCM pile on the lateral load-displacement curve using the best fit parameter from the axial compression pile and comparing it with the observed data from the field test for DCM L-1. The additional parameter used for back analysis is the tensile strength of the DCM material. The tensile strength of the DCM material, TDCM, obtained from the laboratory testing by beam test was 150 kPa while the corresponding values from the lateral pile load test in the field were from 30 kPa to 60 kPa as shown in Fig. 16. Therefore, the simulation of lateral pile load test utilized varying TDCM from 0 to 75 kPa. The TDCM directly affected the yield points of the lateral load versus displacement curves. The higher the TDCM, the higher the ultimate lateral load. The appropriate TDCM is 50 kPa. The TDCM obtained from the simulation agrees with the TDCM derived from the lateral pile load test.

Figure 15(b) shows the results from the simulation compared to the observed data from the field test with SDCM of 0.22×0.22×5.5 m. The other parameter that is significant for the successful performance of the SDCM is the tensile strength of the concrete core pile, T_{core}. The T_{core}, which varied from 4,000 kPa, 5,000 kPa and 6,000 kPa corresponding to 11%, 14% and 17% of the compressive strength of the concrete core pile (35,000 kPa). As shown in Fig. 15(b), the best t parameter of T_{core} is 5,000 kPa for all cases of the SDCM pile.

The 3D FEM model of the full scale test embankment is shown in Fig. 17(a) with 28,950 elements. Figure 17(b) shows that the DCM and SDCM piles beneath the embankment had the same element type and shared the same soil properties as the single pile (see Fig. 12(b)). The settlement versus time comparison between the observed and simulated data from the FEM analysis is plotted in Fig. 18. The settlements from the FEM analysis agreed well with the observed data with regard to both the settlement magnitudes and the settlement rates.

Sensitivity Analysis

A sensitivity analysis was completed to determine the effect of the concrete core length on the ultimate bearing capacities by using different sectional areas as well as lengths of the concrete core pile in numerical experiments. In total, 28 simulations were performed by varying the concrete core pile lengths from 1 to 7 m and varying the sections of square concrete core pile from 0.18 m, 0.22 m, 0.26 m, and 0.30 m, respectively. The summary of the effect of the lengths and sectional areas on the bearing capacities is shown in Fig. 19. The results show that the length of the concrete core pile directly affects the ultimate bearing capacities. Increasing the lengths meant increasing the ultimate bearing capacities. On the other hand, an increase in the sectional areas did not have much impact on the bearing capacities.

The mode of failure of the SDCM and the DCM pile can be investigated by using a relative shear stresses function in 3D FEM simulations. The relative shear stresses give an indication of the

proximity of the stress point to the failure envelope (Brinkgreve and Broere, 2006). It can be defined as the ratio of the shear stress divided by the shear strength. If the relative shear stresses equal 1.0, failure by shear will develop at this point. The comparison of the relative shear strength of the DCM pile and the 2 m, 4 m, 6 m and 7 m length of core pile of the SDCM piles is shown in Fig. 20. Similarly, at the ultimate load, the failure develops about 1 m below the top of the DCM pile and, in the case of SDCM piles, failure develops about 1 m below the tip of the 1 to 6 m long core piles. For the 7 m long core pile of the SDCM pile, the failure took place at the underlying soil stratum. This means that the failure due to shear occurs at a depth of twice the diameter in the DCM pile and 1 to 6 m long core pile of SDCM pile. These failure modes from simulation are similar to the observed failure mode in the full scale tests reported by Zheng and Wu (2005). It can be concluded that, in the case of DCM pile and 1 to 6 m core pile of SDCM pile, the failure developed at the unreinforced part or the DCM piles at about twice the diameter below the tip of core pile (DCM pile failure). On the other hand, in the case of 7 m long core pile in SDCM piles, the failure developed at the soil below SDCM pile (soil failure). Moreover, in the case of 6 m long core pile of SDCM piles, the failure occurred in both the soil and the DCM materials.

The axial load transfer along the pile lengths of the DCM and SDCM pile was different. For the DCM pile, the maximum load developed at the top 1 m and rapidly decreased until a depth of 4 m from the pile top and constant load of 10% of the ultimate load until the tip of the DCM pile (Fig. 21). Thus, the failure took place at the top in the case of DCM pile (see Fig. 1(a)). On the other hand, the axial load at the top of SDCM comprised 90% of ultimate load and linearly decreased to the pile tip, consisting of 70% and 30% of ultimate load and corresponding to 2 m and 7 m of concrete core pile length, respectively (Fig. 22).

A sensitivity analysis was done to determine the effect of the concrete core pile on the lateral loads by varying the lengths of concrete core pile from 0.5 to 6.5 m and also varying the sectional areas of core pile to 0.18 m, 0.22 m, 0.26 m and 0.30 m, as illustrated. These were the same as those used in the axial compression pile test. The effects of the lengths on the ultimate lateral load of the SDCM pile are summarized in Fig. 23. It can be concluded that the results were similar for length of core pile longer than 3.5 m for all sectional areas. The comparison between the FEM simulated results and the measured lateral displacement profile (Figs. 24(a, b)) showed lateral movement with depth. There were slight underestimations of the simulated results for the lateral displacements in DCM pile from 3 m to 8 m depth. The observed lateral movement profiles of SDCM pile were similar in shape to those of the DCM pile obtained from simulations immediately after construction until 570 days after construction.

CONCLUSIONS

This paper presents the observed and simulated results of the full scale embankment loading as well as full scale load tests on soft clay foundation improved by deep cement mixing (DCM) and stiffened deep cement mixing (SDCM) piles. The jet grouting method (jet pressure of 22 MPa) was utilized in the installation of DCM piles with a 0.6 m diameter. The SDCM is a reinforced DCM with a 0.22 m by 0.22 m precast concrete pile inserted at its center. The test results were simulated by a 3D finite element method (FEM) to back-analyze and confirm the related design parameters which were used further in the numerical experiments. Based on the results as well as subsequent analyses and FEM simulations, the following conclusions can be made:

1. By comparing the full scale axial compression load tests on the DCM and SDCM piles, the ultimate bearing capacity of SDCM piles with 0.22 m square and 6 m long concrete core pile can be improved by a factor of between 1.4 and 2 compared to the DCM piles. The low ultimate bearing capacities in the DCM piles can occur due to the non-uniformity of shear strength and the low quality control in the in-situ mixing during construction.

2. By comparing the full scale lateral load tests on the DCM and SDCM piles, the lateral ultimate bearing capacities of the SDCM piles can be increased by up to 15 times. The low lateral resistance of the DCM piles is due to its low flexural strength.

3. By comparing the full scale embankment load test on soft ground improved by the DCM and SDCM piles, the SDCM pile reduced the settlement by 40z and lateral movement by 60z compared to the DCM piles.

4. The strength reduction factor for interfaces, R_{inter}, of 0.40 was obtained from the full scale pullout interface test. Subsequent numerical simulations using the 3D FEM simulations for modeling the interface behavior between the concrete core pile and DCM material in SDCM pile conˆrmed this value.

5. The length of concrete core significantly affected the compression of SDCM pile. In contrast, the sectional area of concrete core only slightly affected the settlement of SDCM pile. The effective value of the length ratio (L_{core}/L_{DCM}) ranges from 0.57 to 0.85 for the compression of the SDCM pile.

6. Both the lengths and cross-sectional area of the SDCM piles influenced its ability to resist lateral pressure. The effective value of the length ratio (L_{core}/L_{DCM}) to resist lateral movement also ranges from 0.57 to 0.85.

7. From the test results and subsequent numerical experiments, including a sensitivity analysis using 3D FEM simulations, the superiority of the new technology called SDCM piles over the traditional technology of DCM piles has been confirmed.

REFERENCES

ASTM D1143-94 (1994): Standard test method for piles under static axial compression load, Annual Book of ASTM Standards.

ASTM D3689-94 (1994): Standard test method for piles under static axial tensile load, Annual Book of ASTM Standards.

ASTM D3966-94 (1994): Standard test method for piles under lateral load, Annual Book of ASTM Standards.

Balasubramaniam, A. S., Hwang, Z. M., Uddin, W., Chaudhry, A. R. and Li, Y. G. (1978): Critical state parameters and peak stress envelopes for Bangkok clays, Quarterly Journal of Engineering Geology, 11, 219–232.

Bergado, D. T., Chai, J. C. and Miura, N. (1995): FE analysis of grid reinforced embankment system on soft Bangkok clay, Computers and Geotechnics, 17, 447–471.

Bergado, D. T., Ruenkrairergsa, T., Taesiri, Y. and Balasubramaniam, A. S. (1999): Deep soil mixing to reduce embankment settlement, Ground Improvement Journal, 3(3), 1–18.

Bergado, D. T., Long, P. V. and Srivinasa Murthy, B. R. (2002a): A case study of geotextile-reinforced embankment of soft ground, Geotextiles and Geomembranes, 20(6), 343–365.

Bergado, D. T., Teerawattanasuk, C., Youwai, S. and Voottipruex, P. (2002b): FE modeling of hexagonal wire reinforced embankment on soft clay, Canadian Geotechnical Journal, 37, 1209–1226.

Brinkgreve, R. B. and Broere, W. (2006): Plaxis 3D Foundation, Version 1.6 Manual, Balkema, A. A., Rotterdam, Brookˆeld, Netherlands.

Butler, H. D. and Hoy, H. E. (1977): The Texas Quick Load Method for Foundation Load Testing—User's Manual, Federal Highway Administration Report, No. FHWA-IP-77-8.

Chai, J. C. (1992): Interaction behavior between grid reinforcement and cohesive frictional soils and performance of reinforced wall/embankment on soft ground, D. Eng Dissertation No. GT-91-1, Asian Institute of Technology, Bangkok, Thailand.

Chen, C. H. (1990): Behavior of the improved ground by deep mixing method underembankment loading, M. Eng. Thesis, Asian Institute of Technology, Thailand.

Dong, P., Qin, R. and Chen, Z. (2004): Bearing capacity and settlement of concrete-cored DCM pile in soft ground, Geotechnical and Geological Engineering, 22(1), 105–119.

Honjo, Y., Chen, C. H., Lin, D. G., Bergado, D. T., Balasubramaniam, A. S. and Okumura, R. (1991): Behavior of the improved ground by the deep mixing method, Proceedings Kozai Club Seminar, Bangkok, Thailand.

Jamsawang, P., Bergado, D. T., Bandari, A. and Voottipruex, P. (2008): Investigation and simulation of behavior of stiŠened deep cement mixing (SDCM) piles, International Journal of Geotechnical Engineering, 2(3), 229–246.

Jamsawang, P. (2009): Full scale tests on stiŠened deep cement mixing (SDCM) including 3D finite element simulation, D. Eng Dissertation, No. GE-08-01, Asian Institute of Technology, Bangkok, Thailand.

Lai, Y. P., Bergado, D. T., Lorenzo, G. A. and Duangchan, T. (2006): Full-scale reinforced embankment on deep jet mixing improved ground, Ground Improvement Journal, 10(4), 153–164.

Lin, K. Q. and Wong, I. H. (1999): Use of deep mixing to reduce settlement at bridge approaches, ASCE Journal of Geotechnical and Geoenvironmental Engineering, 125(4), 309–320.

Petchgate, K., Jongpradist, P. and Panmanajareonphol, S. (2003a): Field pile load test of soil-cement column in soft clay, Proceedings of the International Symposium 2003 on Soil/Ground Improvement and Geosynthetics in Waste Containment and Erosion Control Applications, Bangkok, Thailand, 175–184.

Petchgate, K., Jongpradist, P. and Samanrattanasatien, P. (2003b): Lateral movement behavior of cement retaining wall during construction of a reservoir, Proceedings of the International Symposium on Soil/Ground Improvement and Geosynthetics in Waste Containment and Erosion Control Applications, Bangkok, Thailand, 195–205.

Petchgate, K., Jongpradist, P. and Jamsawang, P. (2004): Field ‰exural behavior of soil-cement column, Proceedings of the Fifth Symposium on Soil/Ground Improvement and Geosynthetics, King Mongkut's University of Technology Thonburi, Thailand, 85–90.

Shinwuttiwong, W. (2007): Full scale behavior of SDCM piles under axial and lateral loading with simulations, M. Eng. Thesis, No. GE-07-04, Asian Institute of Technology, Bangkok, Thailand.

Tand, K. E. and Vipulandan, C. (2008): Comparison of computed vs measured lateral load/de‰ection response of ACIP piles, PLAXIS Bulletin, 23, 10–13.

Terashi, M. and H. Tanaka (1981): Ground improved by deep mixing method, Proceedings of the 10th International Conference on Soil Mechanics and Foundation Engineering, l3, 777–780.

Vermeer, P. A. and Brinkgreve, R. B. J. (1995): Finite Element Code for Soil and Rock Analysis, A. A. Balkema, Rotterdam, Netherlands.

Wu M., Zhao X. and Dou Y. M. (2005): Application of stiŠened deep cement mixed column in ground improvement, Proceedings International Conference on Deep Mixing Best Practices and Recent Advances, Stockholm, Sweden, 463–468.

Zheng, G. and Gu, X. L. (2005): Development and practice of composite DMM column in China, Proceedings 16th International Conference on Soil Mechanics and Geotechnical Engineering, Osaka, Japan, 3, 1295–1300.

Table 1 Soil models and parameters used in 3D FEM simulation

Materials		Model	γ (kN/m^3)	Material behavior	E'_{ref} (kPa)	ν'	λ^*	κ^*	c' (kPa)	ϕ' (deg)	OCR	Tensile Strength (kPa)
Subsoil	Depth(m)											
Weathered crust	0-2.0	MCM	17	Undrained	2500	0.25			10	23		
Soft clay	2.0-8.0	SSM	15	Undrained			0.10	0.020	2	23	1.5	
Medium stiff clay	8.0-10.0	MCM	18	Undrained	5000	0.25			10	25		
Stiff clay	10.0-30.0	MCM	19	Undrained	9000	0.25			30	26		
Foundation												
Concrete core pile		MCM	24	Drained	$2.8\text{x}10^7$	0.15			8000	40		50000
DCM pile		MCM	15	Undrained	30000-	0.33			200-300	30		
(with interface elements)					60000							0-100
Steel plate		LEM	-	Non-porous	$2.1\text{x}10^8$	0.15						

SSM: soft soil model; MCM: Mohr-Coulomb model; LEM: linear elastic model

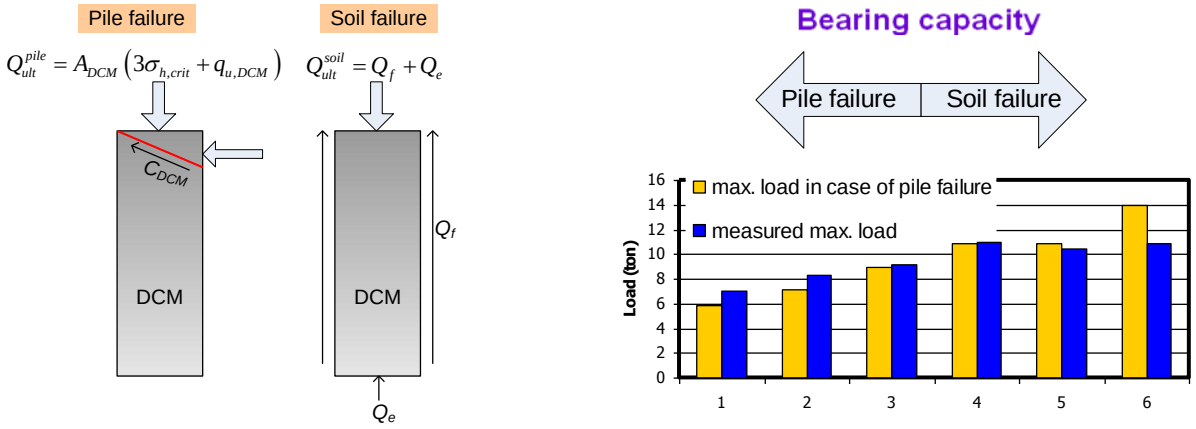

Fig. 1 Low quality of DCM piles on Soft Bangkok Clay (Petchagate et al., 2003a, b)

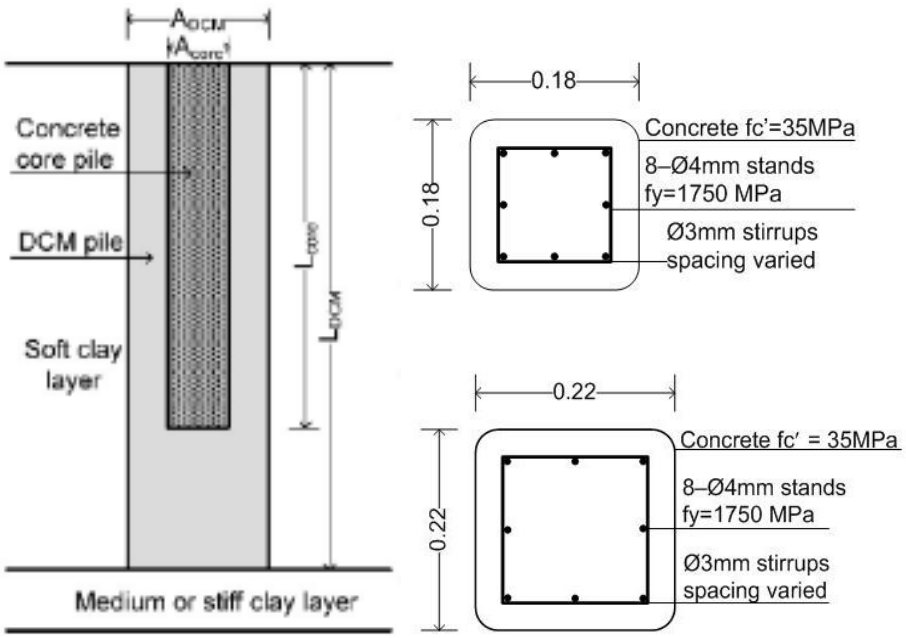

Fig. 2. Schematic of SDCM and the details of pre-stressed concrete core piles

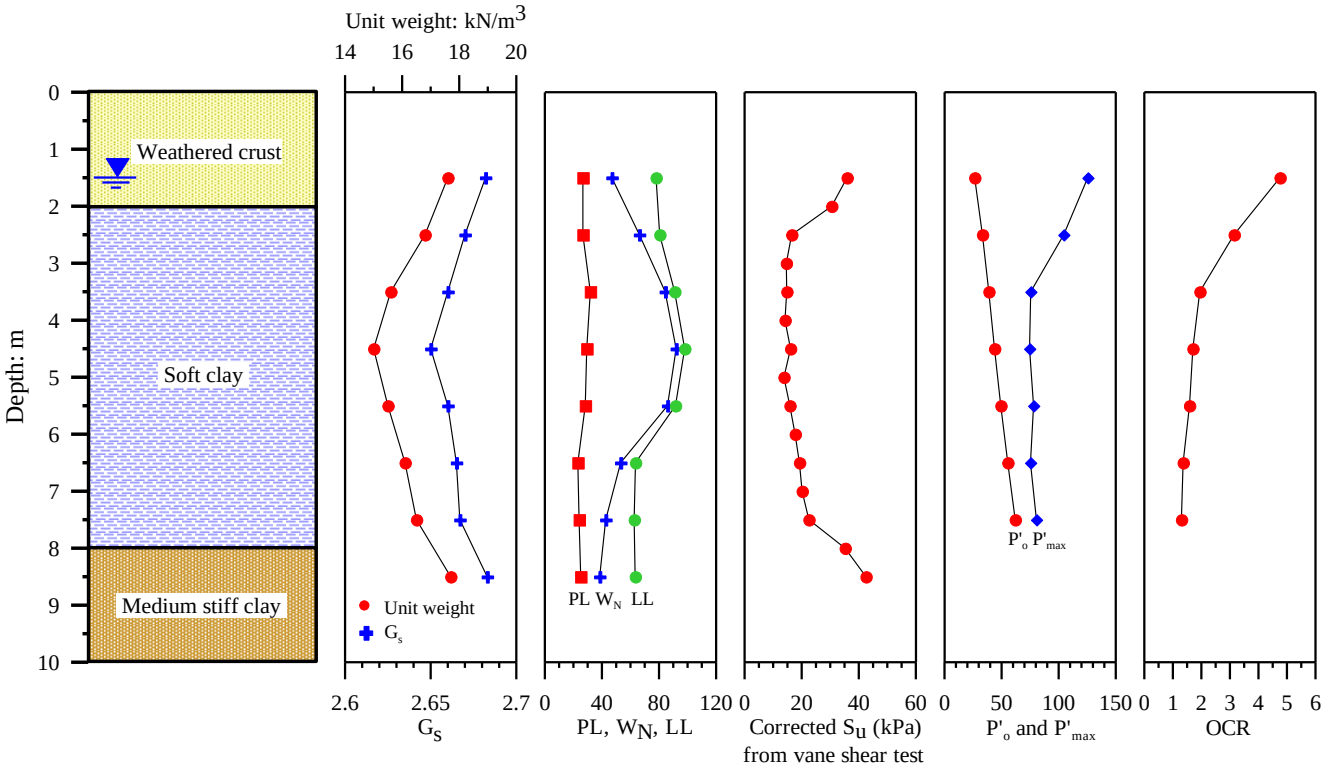

Fig. 3. Subsoil profile and relevant parameters

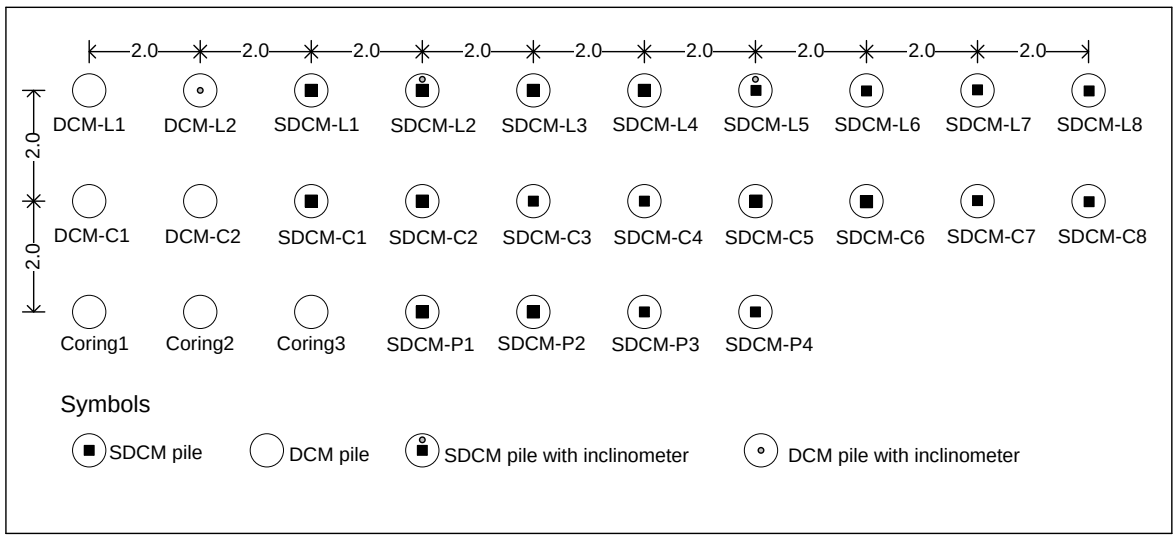

Fig. 4 Pile load test layout

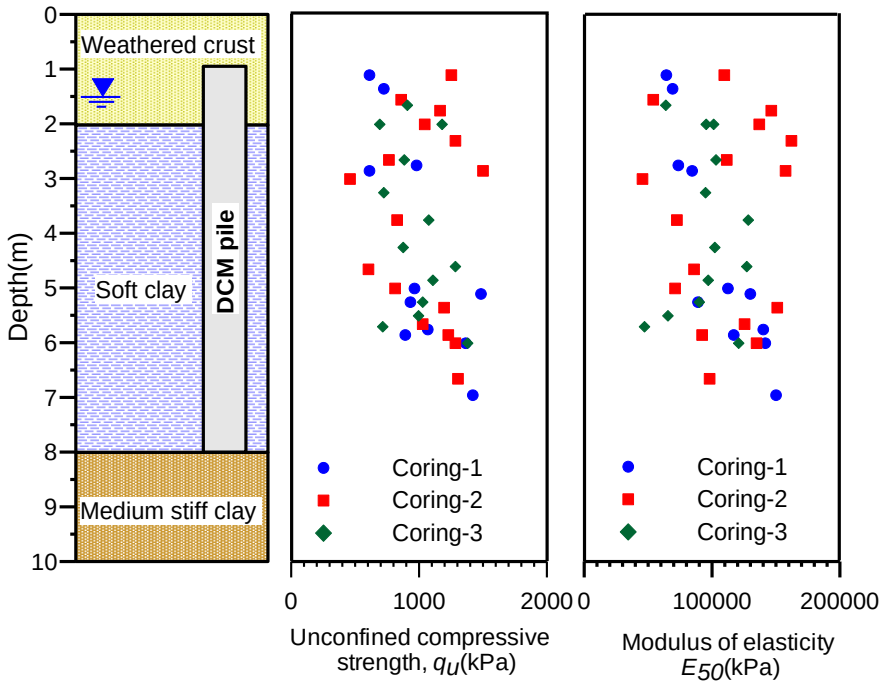

(a) Engineering properties of DCM piles

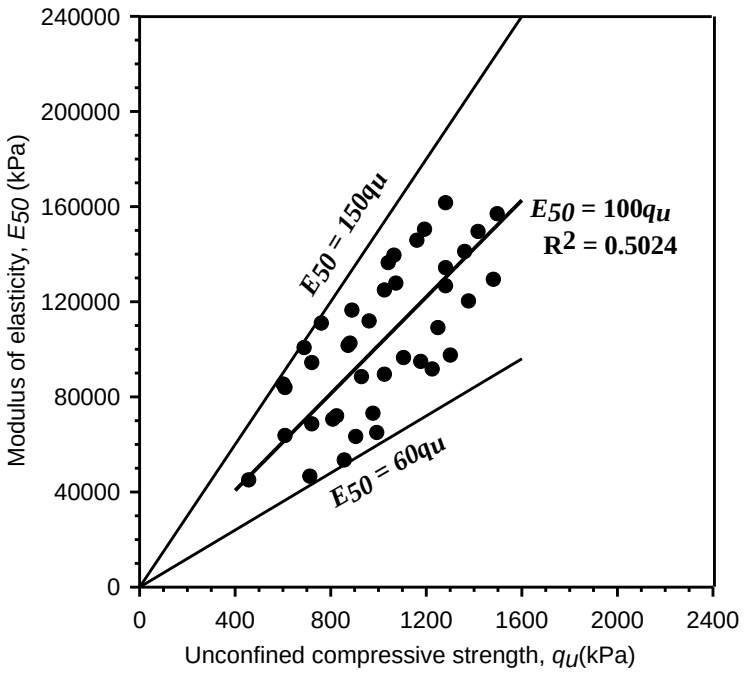

(b) Relationship between E_{50} and q_u of DCM pile

Fig. 5. Field test results on DCM piles

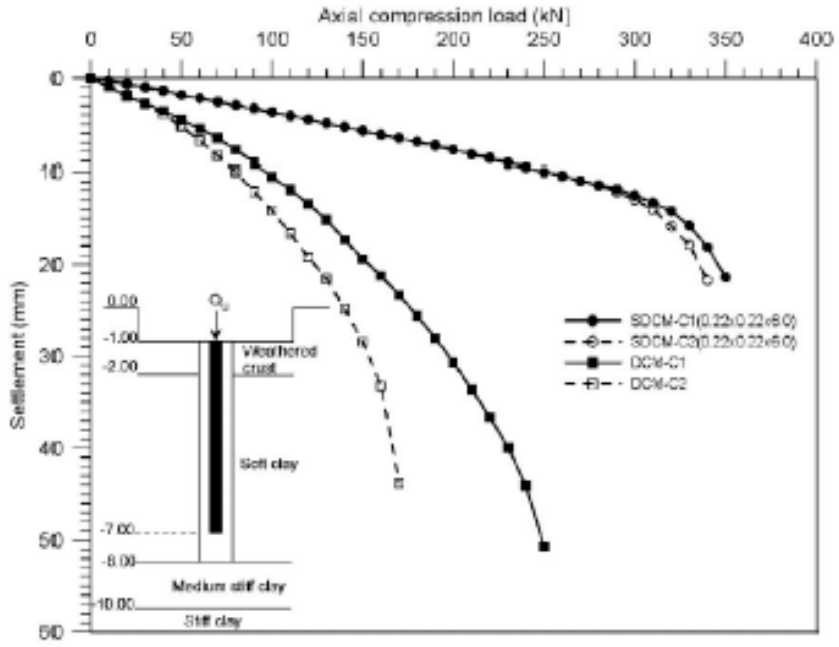

Fig. 6 Axial Compression load settlement curve

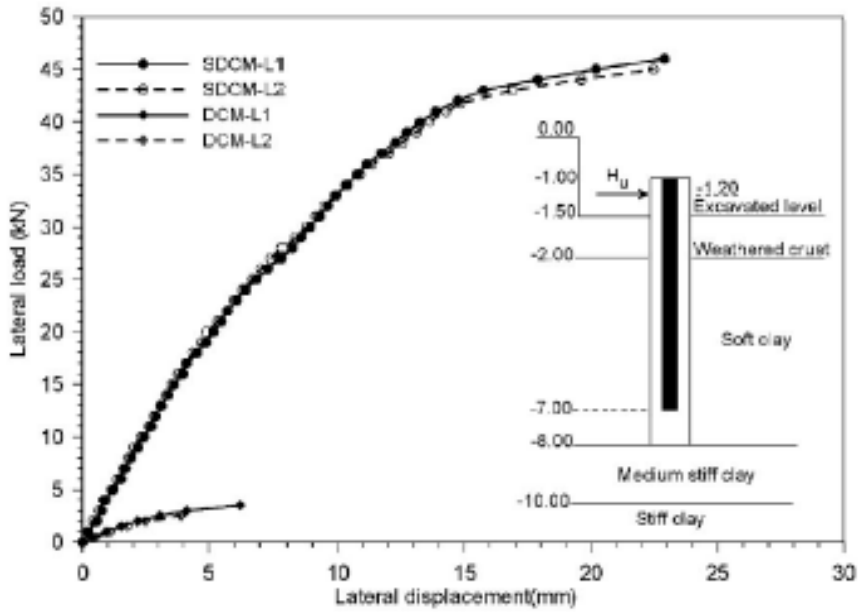

Fig. 7 Lateral load – lateral displacement curve

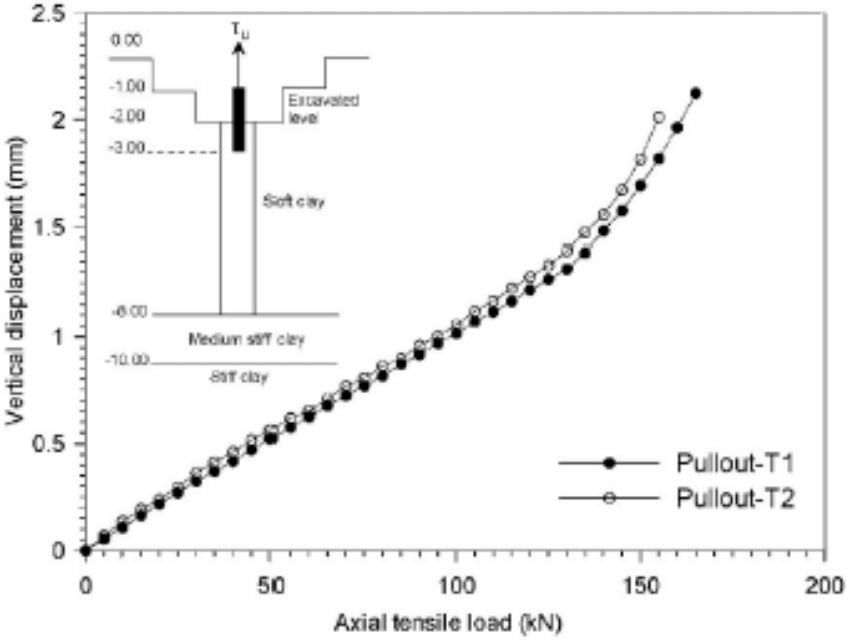

Fig. 8 Tensile load –vertical displacement curve

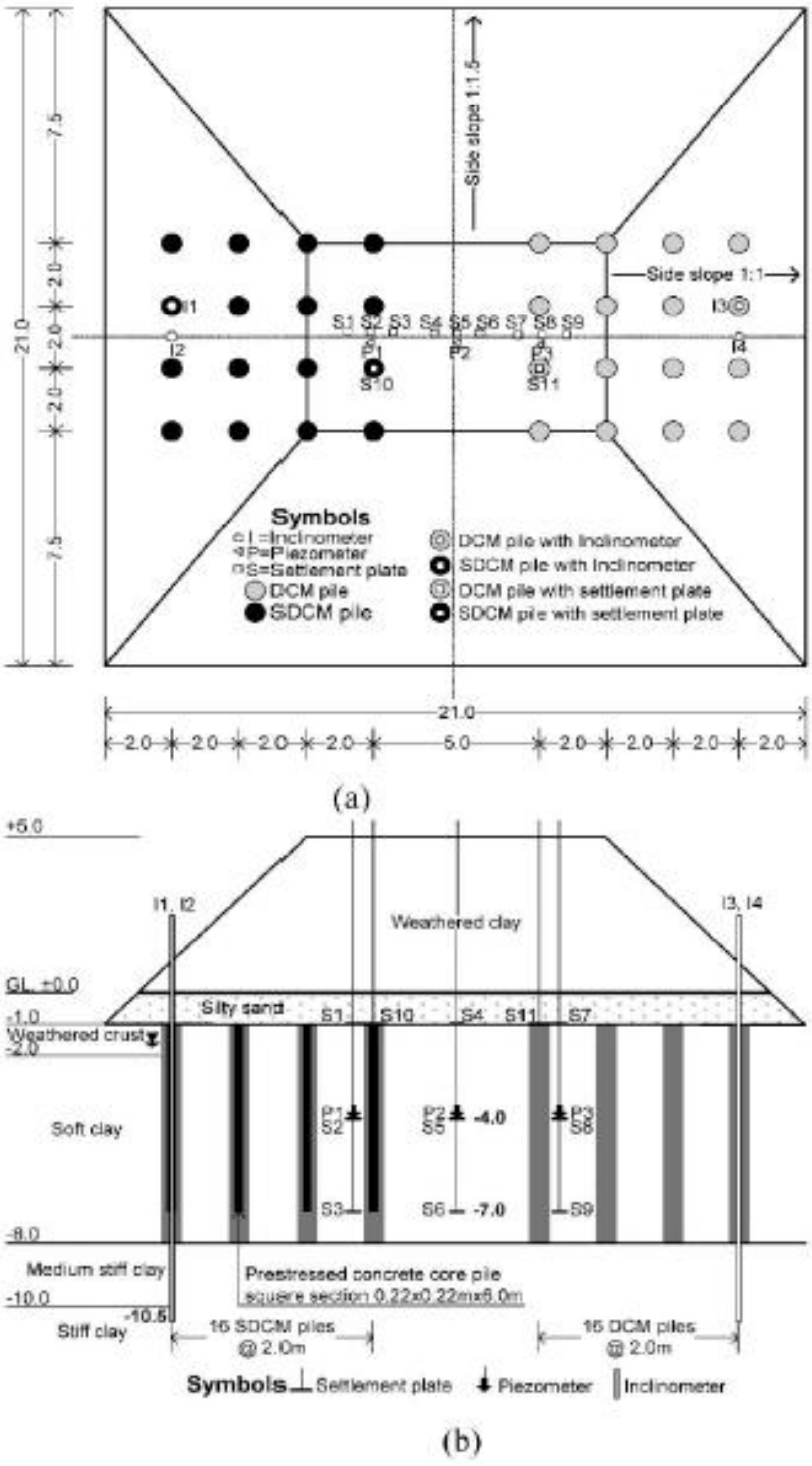

Fig. 9 (a)Plan view of test embankment on SDCM and DCM pile (b)Cross section of test embankment on SDCM and DCM piles

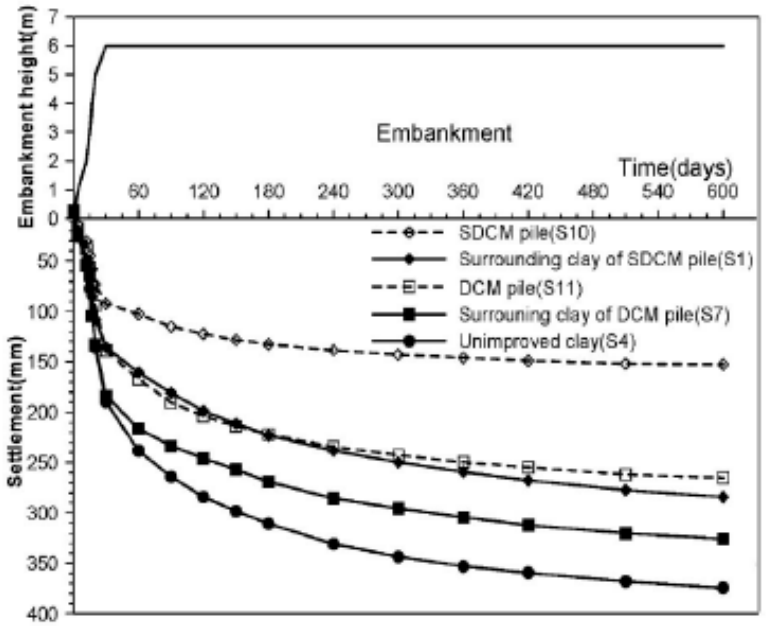

Fig. 10 Comparison of surface settlements

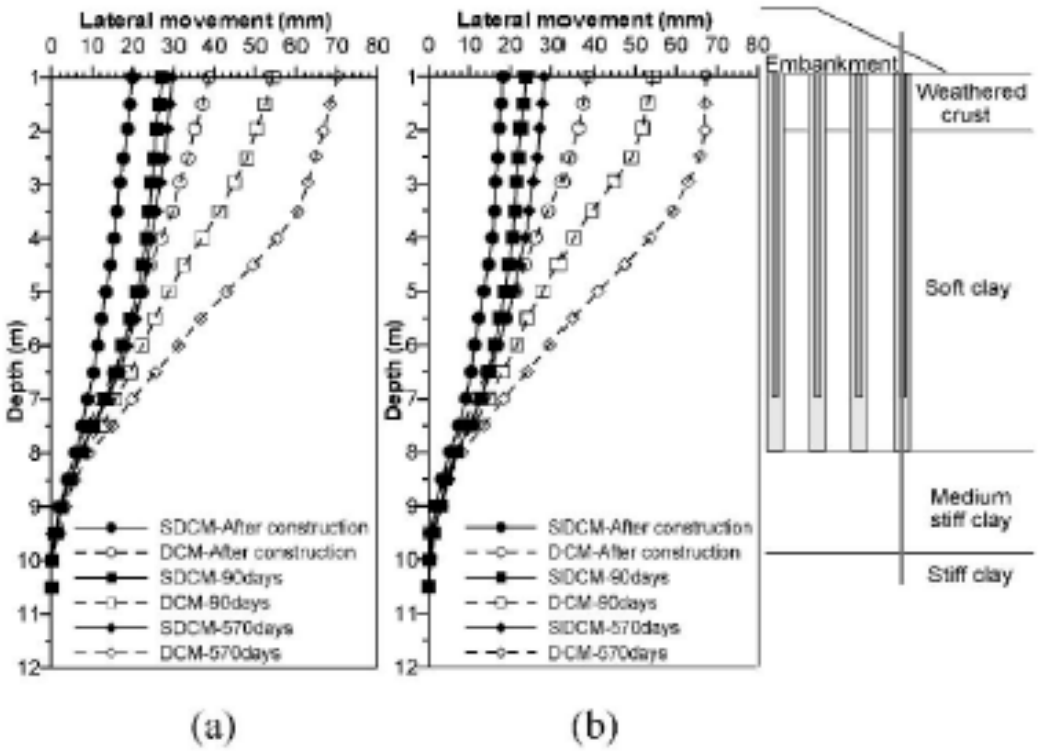

Fig 11 (a) Laterla movement profiles SDCM and DCM piles (b) Lateral movement profiles of surrounding clay of SDCM and DCM piles

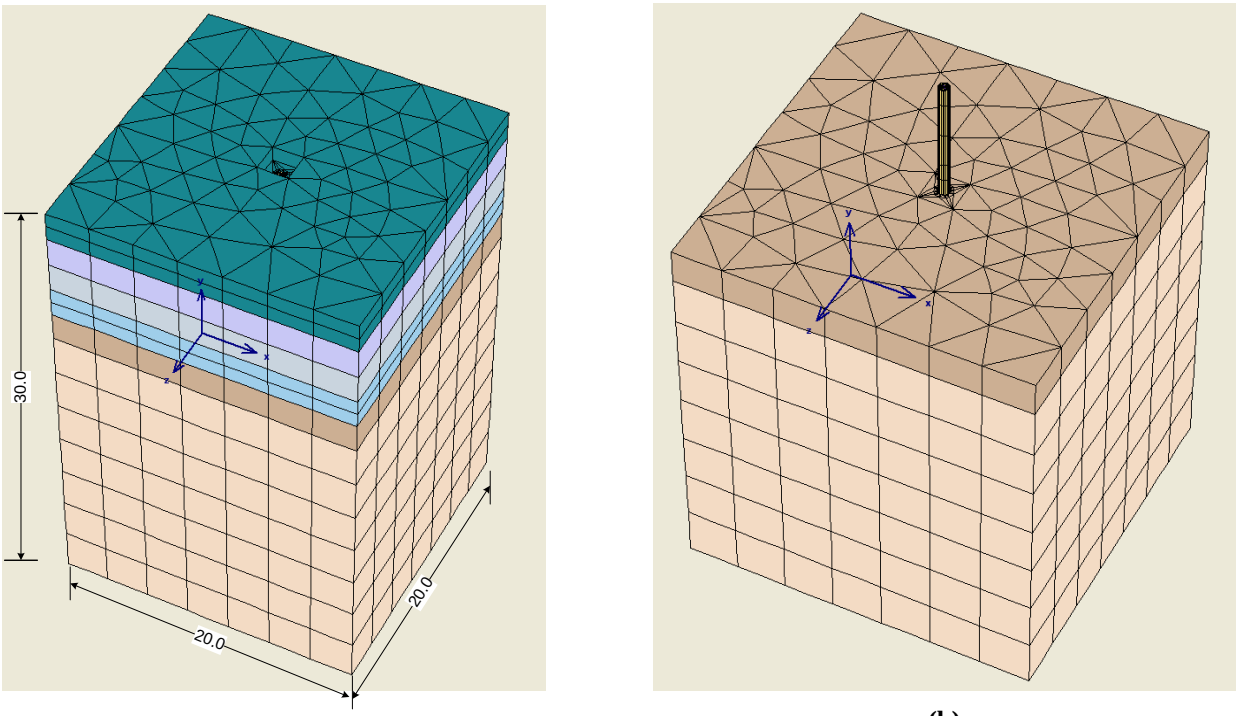

(a) **(b)**

Fig. 12 Portion of 3D FEM model of pile test, (b) Portion of 3D FEM model of SDCM and DCM piles

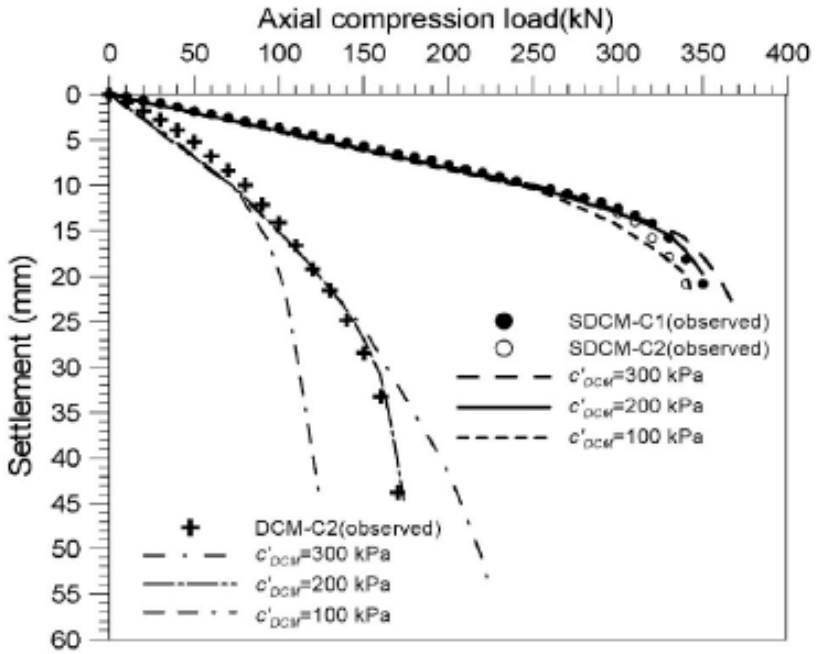

Fig. 13 Effect of cohesion of DCM pile on axial compression load settlement curve

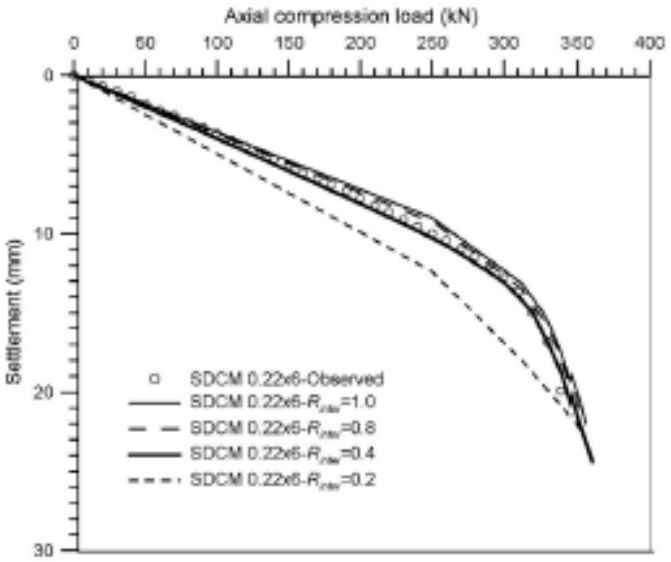

Fig. 14 Effect of R_{inter} on axial compression load-settlement curves for SDCM piles with 0.22 m square and 6 m long concrete core pile

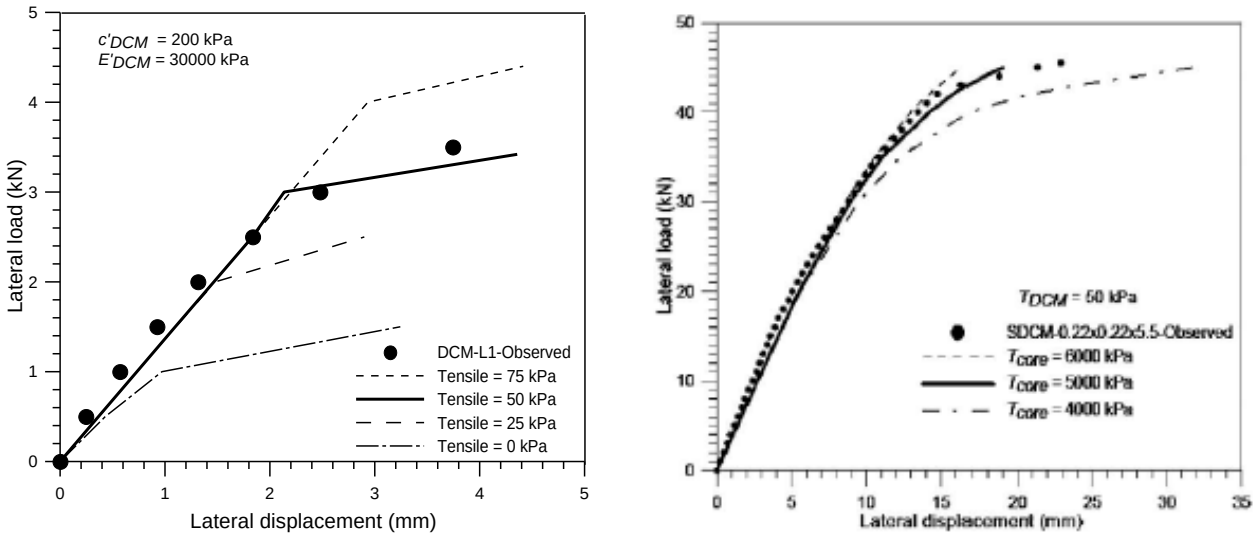

Fig. 15 Effect of tensile strength of DCM pile on lateral load –lateral displacement curve (a) DCM-L1 and (b) SDCM piles

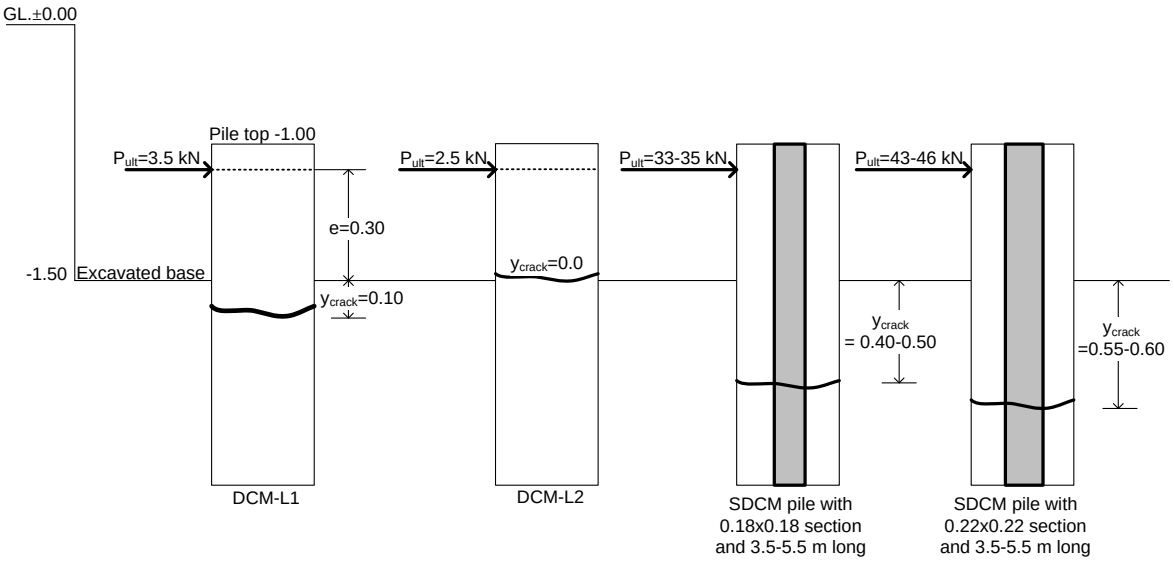

Fig. 16 Mode of failure of DCM and SDCM piles under lateral loading tests

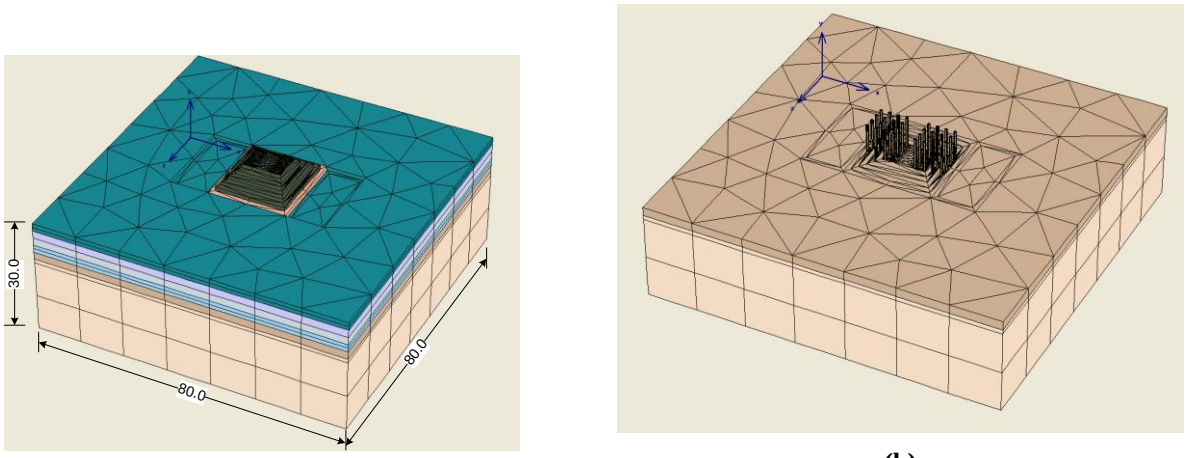

(a) **(b)**

Fig. 17 Portion of 3D FEM model of embankment, (b) Portion of 3D FEM model of SDCM and DCM piles

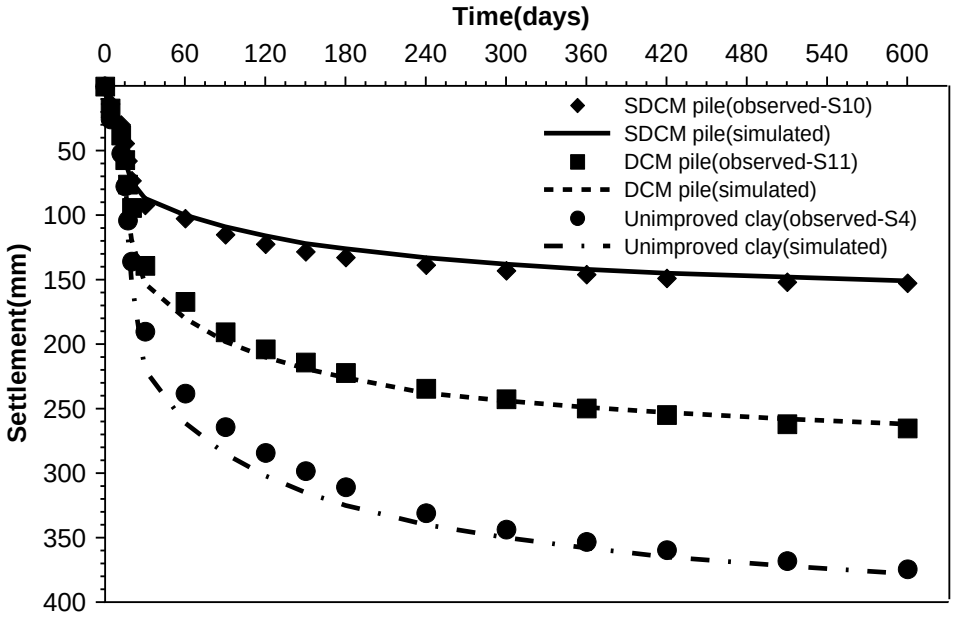

Fig. 18 Surface settlements from simulation

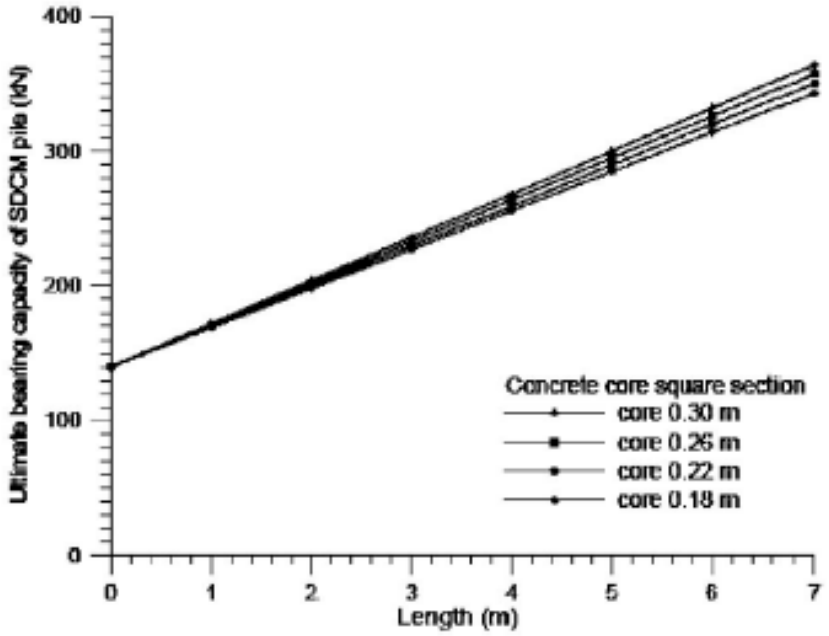

Fig. 19 Effect of lengths and sectional areas of concrete core piles on ultimate bearing capacity

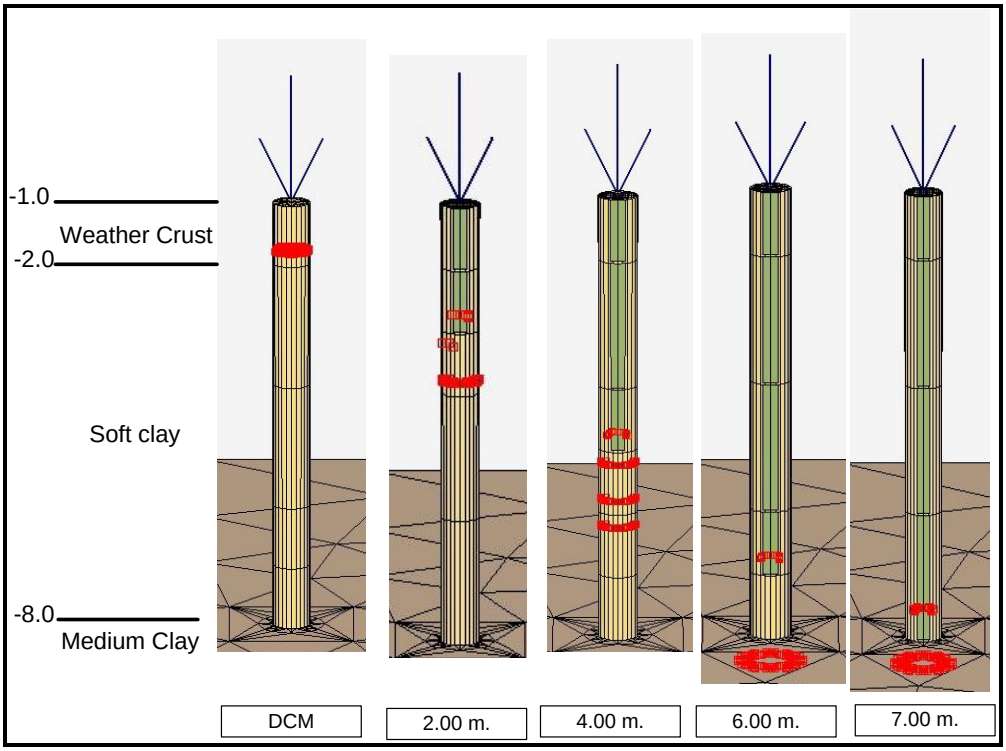

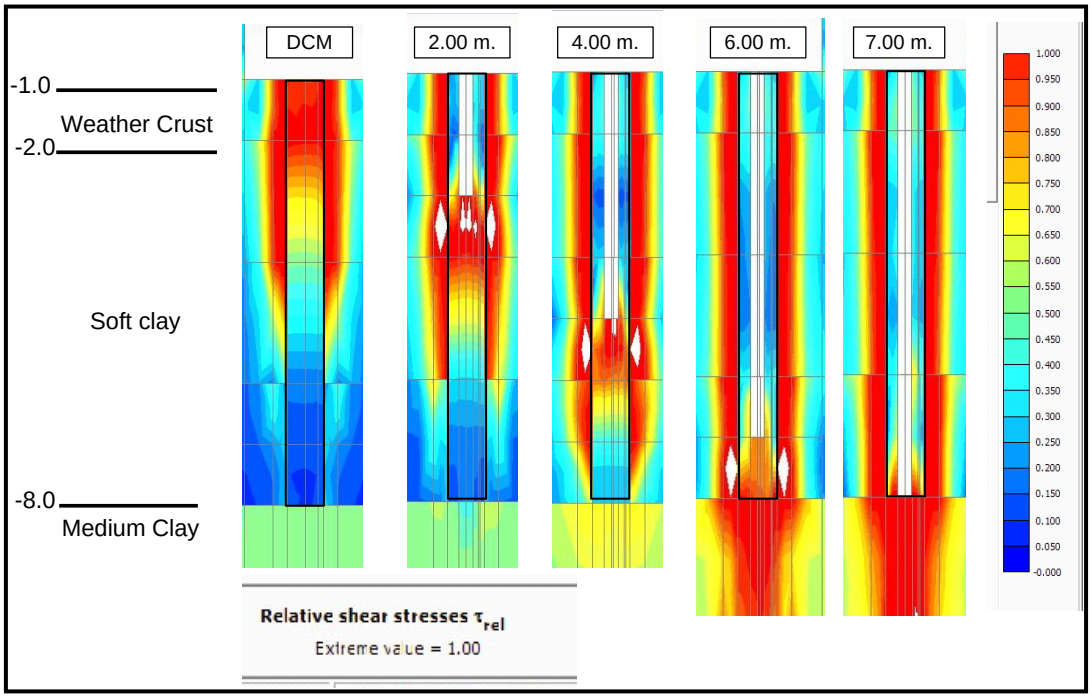

Fig. 20 Relative shear stresses of 0.22 x 0.22 core piles at failure load from simulations

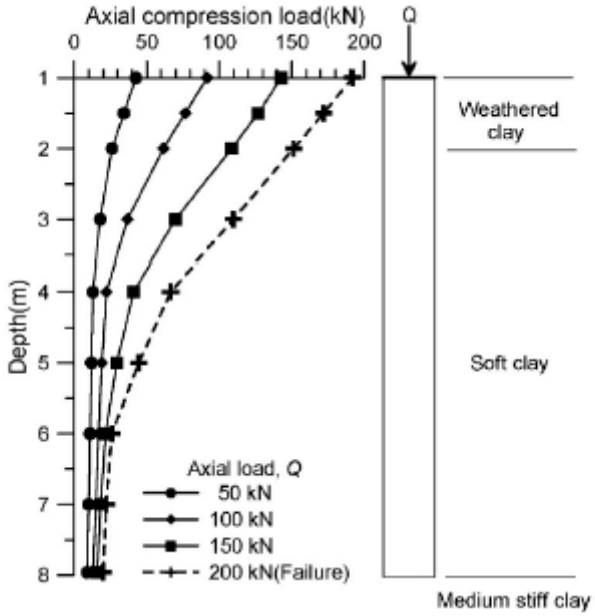

Fig. 21 Axial load distribution along DCM-L1 from simulation

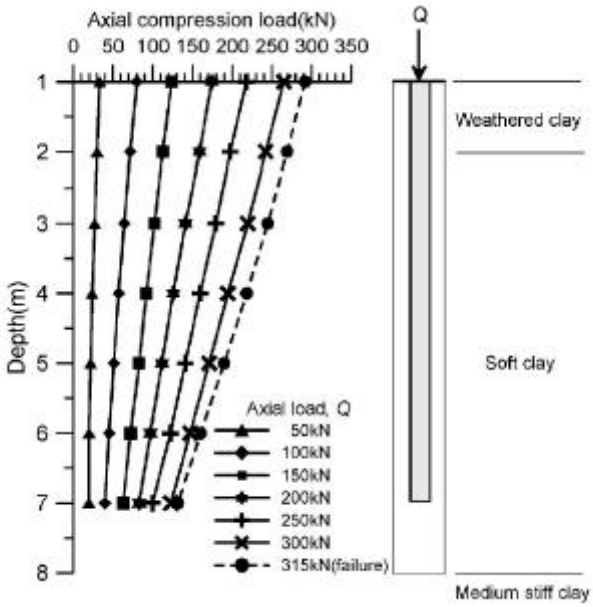

Fig. 22 Axial load distribution along 0.22 x 0.22 x 6 m from simulation

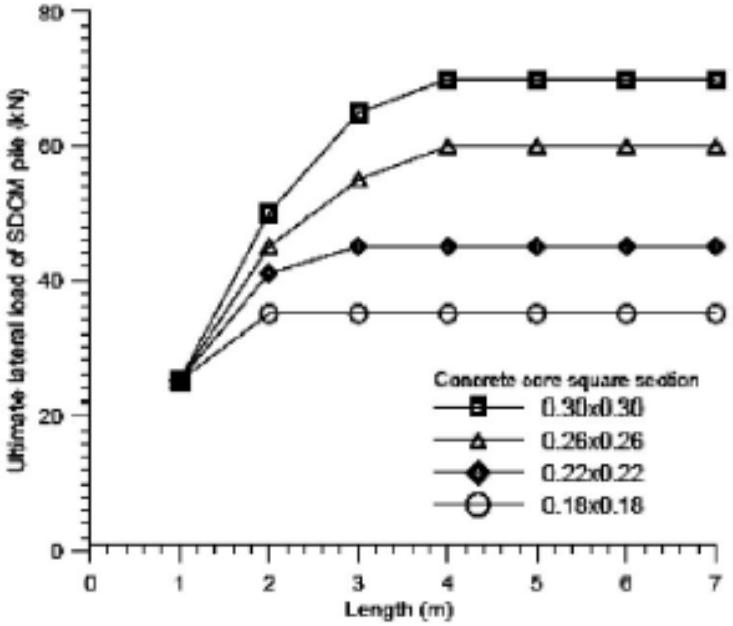

Fig. 23 Effect of lengths and sectional areas of concrete core piles on the ultimate lateral load of SDCM pile

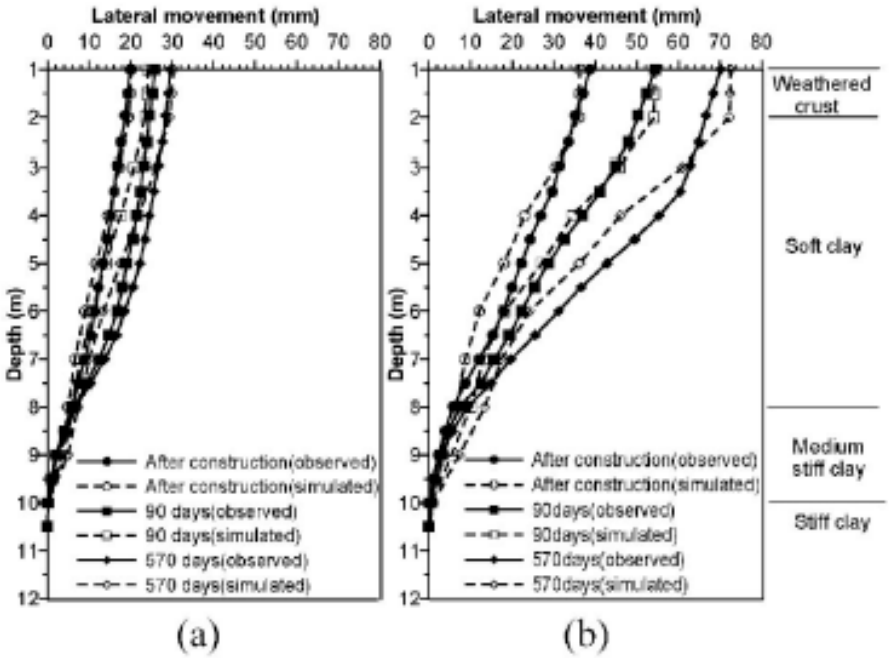

Fig. 24 (a)Lateral movement profiles of SDCM pile from simulation (b)Lateral movement profiles of DCM piles from simulation

Use of the observational approach in design and construction of road embankment on soft grounds

H. S. Thilakasiri, Department of Civil Engineering, University of Moratuwa

Abstract

Due to the high variability of the soft ground conditions encountered in construction of road embankments, an initial design using unfavourable or prismatic ground conditions becomes uneconomical or sometimes not feasible. Therefore, very often most probable or more optimistic ground conditions are considered in the initial design and the risks associated with such assumptions are managed by reviewing the initial design through observational data obtained during the construction stage. In this paper, the fundamental concepts behind the observational approach of design are discussed. In addition, the uncertainties associated with the properties of soft soil in Sri Lanka are highlighted and the use of the common analytical methods in analysing observational data from road embankments over soft grounds is investigated.

1.0 Introduction

Road traces are very often run through low-lying grounds with soft soil deposits in the subsurface to minimize issues related to compensation and resettlement. This has been often the case with new road embankments constructed in the highly populated western coastal belt of Sri Lanka. Even though running new road traces through such grounds minimizes certain social issues, construction of high road embankment on such weak compressible grounds to avoid flooding is a major challenge faced by geotechnical engineers. The stability of the road embankment on very weak ground is a very serious concern during the construction stage of the embankment and the post construction secondary consolidation settlements pose serious questions regarding the long term serviceability of the road embankment constructed over such soft soil deposits.

The spatial variability of the properties of the soft soil over a wide range is a major problem faced by the designers of road embankment over such ground conditions in Sri Lanka. On the other hand reliable mathematical models predicting the behaviour of the soft soil in Sri Lanka or the properties associated with such models are yet to be revealed through research programmes. As a result, it has become a very difficult task to predict the behaviour of soft soil under road embankment during design stage with sufficient confidence level. Due to the limited understanding and the knowledge of the soft soil, road embankments constructed over soft soil deposits are instrumented and monitored during the construction stage to minimize the risk of failure. This method is commonly known as the 'observational approach'. In this paper, the fundamental concepts and the proper application of the observational approach related to design and construction of road embankments over soft soil deposits are discussed.

2.0 Observational approach

In present day geotechnical engineering, two design approaches are used: conventional approach; and observational approach. In the conventional design approach, the design is finalized before the start of the construction process. Any monitoring carried out during the construction stage will merely be used to check whether the original design falls within the acceptable limits but no contingency measures are incorporated in the design if the original assumptions are not satisfied. Normal design of pile foundations is a commonly known conventional design. The results of the post construction load testing of such piles will be mainly used to check the validity of the designed carrying capacity of piles. However, in the original design no remedial measures for violation of the design assumptions are studied or proposed. Due to this 'rigid approach' used in the conventional designs, the designer tends to minimize the probability of failure by using conservative material parameters

(or most pessimistic or unfavourable material parameters) and conservative analysis options resulting in costly designs.

In the observational approach 'most probable design parameters' are used in contrary to the conservative prismatic design parameters used in the conventional design approach. Eventhough the observational approach had been practiced by engineers over a long period of time, this design approach was first formally introduced by Terzaghi and Peck (1967) as observational procedure. Later Peck (1969) laid down some guidelines for the implementation of the observational design approach. As the 'most probable design' parameters are used, the probability of failure is higher than the same with the conservative approach using pessimistic material parameters. To minimise the probability of failure, the initial design is refined based on the observations obtained from field monitoring and hence, the name observational approach. In this approach the design extends well into the construction phase and the original design is continuously reviewed using the field observations. It is very clear that the observational approach requires field monitoring of the performance of the embankment, analysis of field monitoring data and review of the original design accordingly.

Observational approach provides viable solutions to many geotechnical engineering problems where conventional design approach may require highly conservative assumptions due to uncertainty associated with the natural ground conditions. The uncertainties of the natural ground condition may arise due to two reasons: uncertainties of the variability of soil properties; and the uncertainty associated with insufficient knowledge of the soil properties. The first types of uncertainties commonly referred to as 'aleatoric' uncertainties, are due to the space and time variability of soil properties of a more or less homogeneous soil medium. The second types of uncertainties, referred to as 'epistemic' uncertainties, are due to the lack of the understanding or the behaviour of the soil properties across a site. Uncertainties may be mathematically quantified using probabilistic approach and result in adverse consequences. The 'risk' is defined as the quantified measure of the consequences of an event with the probability of its occurrence. The basic principle behind the implementation of the observational approach is the limiting the risk associated with the uncertainties of the ground conditions by making use of the observed performance of the structure itself during the construction stage.

Peck (1969) identified following eight ingredients for successful implementation of the observational approach:

i. Exploration sufficient to establish at least the general nature, pattern and properties of the deposits, but not necessarily in detail;
ii. Assessment of the most probable conditions and the most unfavourable conceivable deviations from these conditions;
iii. Establishment of the design based on a working hypothesis of behaviour anticipated under the most probable conditions;
iv. Selection of quantities to be observed as construction proceeds and calculation of their anticipated values on the basis of the working hypothesis;
v. Calculation of the values of same quantities under the most unfavourable conditions compatible with the available data concerning the subsurface conditions;
vi. Selection in advance a course of action or modification of design for every foreseeable significant deviation of the observational findings from those predicted on the basis of the working hypothesis;
vii. Measurement of quantities to be observed and evaluated on actual conditions; and
viii. Modification of design to suit actual conditions.

With the advent of the risk assessment practises to engineering design, the use of the most probable ground condition in the design was scrutinized by various researches and different approach for

selection of the initial ground condition were proposed. Eurocode 7 briefly deals with the observational method under clause 2.7 as follows:

i. When prediction of geotechnical behaviour is difficult, it can be appropriate to apply the approach known as "the observational method", in which the design is reviewed during construction.
ii. The following requirements shall be met before construction is started:
    a. acceptable limits of behaviour shall be established;
    b. the range of possible behaviour shall be assessed and it shall be shown that there is an acceptable probability that the actual behaviour will be within the acceptable limits;
    c. a plan of monitoring shall be devised, which will reveal whether the actual behaviour lies within the acceptable limits;
    d. the monitoring shall make this clear at a sufficiently early stage, and with sufficiently short intervals to allow contingency actions to be undertaken successfully;
    e. the response time of the instruments and the procedures for analysing the results shall be sufficiently rapid in relation to the possible evolution of the system;
    f. a plan of contingency actions shall be devised, which may be adapted if the monitoring reveals behaviour outside acceptable limits.
iii. During construction, the monitoring shall be carried out as planned.
iv. The results of the monitoring shall be assessed at appropriate stages and the planned contingency actions shall be put into operation if the limits of behaviour are exceeded.
v. Monitoring equipment shall either be replaced or extended if it fails to supply reliable data of appropriate type or in sufficient quantity.

3.0 Observational approach for construction of road embankment over soft soil deposits

3.1 The initial design

The 'risk', as mentioned previously associated with any events, is a measure of its consequences and the probability of occurrence. Let us know look at the events that may arise due to uncertainty associated with the initial design of the embankment over soft soil deposits and the consequences of such events on achieving the overall project objectives. The events that are of importance may be divided into two categories: events that may occur during construction; and the events that may occurred during post construction stages. As most of the soft soil deposits are normally consolidated, the stability of the sides of the embankment is critical during initial loading stages. Therefore, one event that may arise due to uncertainties associated with the initial design is the failure of the slopes of the embankment during construction stage. One has to analyse the probability of occurrence of such events and the consequences of such events on the overall construction programme.

3.1.1 Uncertainties associated with the stability of the embankment

The probability of slope failure depends on the uncertainty of the soil properties and layering used, and the uncertainty associated with the method of analysis used in the initial design. If one uses the observational approach and the 'behaviour anticipated under the most probable conditions' as stipulated by Peck (1969), there is about 50% probability that actual condition may deviate from the 'most probable' conditions. In an initial design with low safety margin, the probability of occurrence of slope failure may be high.

To quantify the above discussion, let us assume that the there is uncertainty associated with undrained shear strength of the soft soil layer as the reported strengths varies from 6 to 60 kPa with the most probable value as 20 kPa. In a conventional design, the design strength will be taken close to the lower limit and the slopes of the embankment should have a reasonable factor of safety, say 1.3, against failure. However, a design using observational approach may be carried out by assuming an initial design strength of 20 kPa and a factor of safety of 1.3 against the short term failure. One has to now look at the factor of safety when the undrained shear strength is closer to the lower limit of the above range. Does the FoS fall below 1.0 and what is the probability of occurrence? Can that probability of failure be reduced by observing the behaviour of the embankment and taking appropriate remedial actions during the construction stage?

To illustrate some uncertainties associated with the selection of the strength parameters of soft soils in the initial design, undrained shear strength data obtained from field and laboratory testing of natural peaty soils from the Colombo Katynayake Exressway project (CKE), as reported by Hsi et al. (2005), are give in Figure 1. Apart from the spatial variability of S_u there is some discrepancy in the S_u variation from triaxial tests and vane shear tests as well.

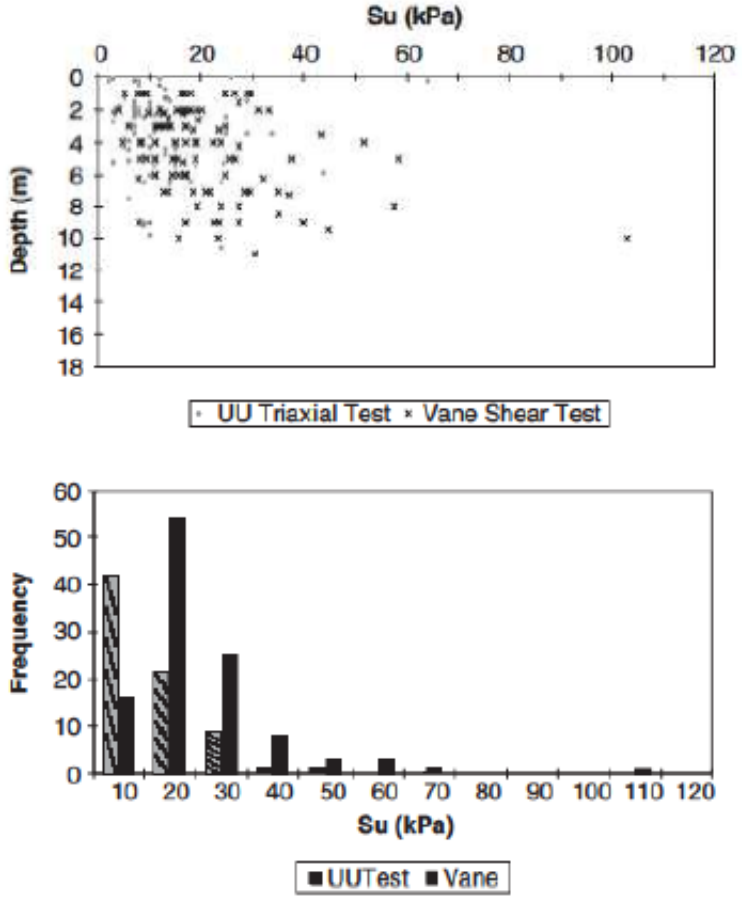

Figure 1 – Variation of the undrained shear strength (S_u) of natural peaty deposits along the CKE trace (Hsi et al., 2005).

There is sufficient evidence to suggest that strength gain of peaty soils is considerable during embankment construction. Ariyarathna and Thilakasiri (2010) presented the strength gain of peaty soil from Sothern Transport Development Project STDP as given in Table 1. It is evident from data presented in Table 1 that the undrained cohesion (c_u) of peaty soils increases with the pre-consolidation pressure (P_c) in the rage of 0.24 to 0.49.

Table 1 – Strength gain of peaty soils from STDP Ariyarathna and Thilakasiri (2010)

Location	P_c (kPa)	c_u (kPa)	c_u / P_c	Location	P_c (kPa)	c_u (kPa)	c_u / P_c
45+405	180.0	79.00	0.44	C1 - 1	200.0	53.20	0.27
	160.0	57.00	0.36		133.0	39.00	0.29
A1 - 1	153.0	57.00	0.37	C1 - 2	140.0	56.25	0.40
A1 - 2	150.0	73.00	0.49		160.0	38.40	0.24
A2	205.0	55.00	0.27	52+970	150.0	41.50	0.28
	200.0	70.00	0.35		170.0	38.25	0.23
B2 - 1	230.0	89.40	0.39	53+690	170.0	54.00	0.32
B2 - 2	240.0	75.40	0.31		147.0	50.50	0.34

Hsi et al. (2005) presented the variation of the undrained shear strength of peaty soils, given in Figure 2, obtained from testing of samples under already constructed embankments of the CKE project. Comparison of the undrained shear strength of natural peaty deposits, given in Figure 1, and the same for consolidated peaty deposits, shown in Figure 2, it is clear that there is clear increment in the undrained strength of peaty soils due to increase in the pre-consolidation pressure.

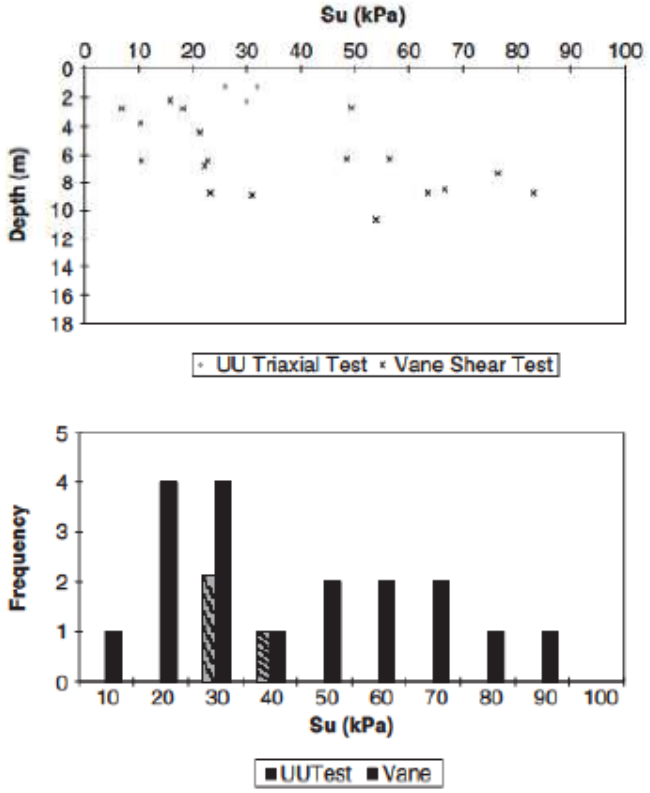

Figure 2 - Variation of the undrained shear strength (S_u) of peaty deposits under the embankments of the CKE trace (Hsi et al., 2005).

The significance of the strength gain in the initial design is illustrated by carrying out stability analysis of an embankment constructed over soft soil deposits with and without strength gain effects. Results of the parametric study carried out are shown in Table 2. In the parametric study construction of a typical 8m high embankment over a 9.7m thick soft soil layer was considered and a typical failure surface is shown in Figure 3. Embankment over untreated peaty soil and peaty soil layer treated with 0.5m diameter sand compaction pile (SCP) at 1.4m spacing in an equilateral triangular configuration were considered in the parametric study. Angle of internal friction of the SCP is assumed to be 32^0 and the equivalent material properties of the soft soil deposit based on the area ratio of the SCP was used in the slope stability analysis. Table 3 shows the variation of the FoS of the embankment slope with the height of the embankment constructed in 8 step loading stages. The

degree of consolidation of 50% under the already placed weight of the embankment is assumed before placing each loading step.

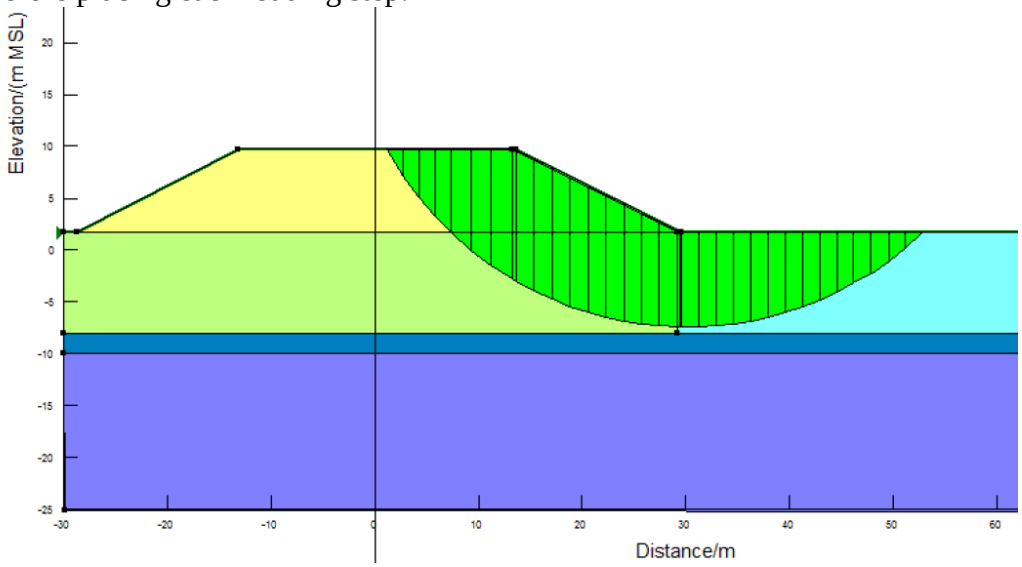

Figure 3 – Typical circular failure surface obtained during the parametric study.

Table 2 – Variation of the FoS against slope failure depending on the treatment of SCP and strength gain effect.

Description	Lift height(m)	Degree of Consolidation	Stremgth gain ratio	Region 1		Region 2		FOS				
				c_u	φ	c_u	φ	M-P	Janbu	Bishop	Ordinary	MIN
Application of Total load without any treatment	8	0	0	12	0	12	0	0.53	0.50	0.53	0.53	0.50
Application of Total load without any treatment and considered 50% consolidation under full load	8	50	0.3	34.8	0	12	0	1.03	0.96	1.04	0.98	0.96
Application of Total load with SCP without strength grain	8	0	0	10.6	3.6	12	0	0.74	0.70	0.75	0.70	0.70
Application of Total load with SCP and considered 50% consolidation under full load	8	50	0.3	30.8	3.6	12	0	1.14	1.06	1.15	1.06	1.06

Table 3 – Variation of the FoS of the embankment with the height of the embankment during step loading

Description	Lift height(m)	Degree of Consolidation	Stremgth gain ratio	Region 1		Region 2		FOS				
				c_u	φ	c_u	φ	M-P	Janbu	Bishop	Ordinary	MIN
Stage construction without SCP	1	0	0	12.0	0	12	0	3.77	3.56	3.77	3.74	3.56
Stage construction without SCP	2	50	0.3	14.9	0	12	0	2.02	1.86	2.03	1.95	1.86
Stage construction without SCP	3	50	0.3	17.7	0	12	0	1.59	1.46	1.60	1.50	1.46
Stage construction without SCP	4	50	0.3	20.6	0	12	0	1.33	1.26	1.33	1.29	1.26
Stage construction without SCP	5	50	0.3	23.4	0	12	0	1.18	1.11	1.18	1.14	1.11
Stage construction without SCP	6	50	0.3	26.3	0	12	0	1.09	1.02	1.09	1.04	1.02
Stage construction without SCP	7	50	0.3	29.1	0	12	0	1.02	0.95	1.02	0.97	0.95
Stage construction without SCP	8	50	0.3	32.0	0	12	0	0.96	0.90	0.97	0.92	0.90

It is clearly seen that there is a significant effect of the strength gain on the FoS against embankment failure. In the results presented in Tables 2 & 3 it is assumed that the soft soil has attained a degree of consolidation of 50% under the already placed embankment load. However, in an actual design the degree of consolidation should be estimated based on the embankment filling rate and the consolidation characteristics of the soft soil deposit. There is some uncertainty associated with the models available to obtain the degree of consolidation of the soft soil deposits. In addition, even though it is assumed in the above analysis that the strength gain factor is constant at 0.3, there is considerable variation in the observed strength gain factors given in Table 1. The strength gain effects of cohesive soils are generally quantified by the relationship given in Equation [1]. However, the applicability of this relationship for Sri Lankan peaty soils is not yet proved through a reliable research programme.

$$\frac{\Delta c_u}{\Delta \sigma_v^{/}} = 0.11 + 0.0037PI \qquad [1]$$

Where Δc_u and $\Delta \sigma_v^{/}$ are the increase in the undrained strength and the effective vertical stress on the cohesive soil and *PI* is the plasticity index of the soft cohesive soil.

In the observational approach, if significant deviation of the observational findings from those predicted on the basis of the working hypothesis is noted, appropriate predetermined contingency measures should be carried out. Such contingency measures may require additional financial resources and may result in delays in the overall project duration. Therefore, the amount of risk has to be managed depending on how the additional time and cost associated with probable contingency measures can be absorbed into the overall management of the project. Therefore, establishment of the initial design based on a working hypothesis of behaviour anticipated under the most probable conditions as stipulated by Peck (1969) has to be looked at in the context of individual project and the constraints associated with it.

3.1.2 Uncertainties associated with the serviceability state of the embankment

The other aspect that has to be looked at is the long term performance of the embankment. In this context the post construction settlement and differential settlement is a main concern. The time period over which the embankment load should be kept before the construction of the road pavement, referred here as the preloading duration, is one factor that will have a certain effect on the long term performance of the embankment. In addition, the soft soil under the embankment is surcharged to achieve a certain overconsolidation ratio during the service life of the embankment to reduce the long term secondary consolidation settlement. The preloading duration should be determined during the initial design using appropriate primary and secondary consolidation models and the embankment construction should be carried out accordingly.

Consolidation parameters obtained from laboratory consolidation tests play a very important part in this context. Table 4 shows the variability of consolidation parameters of natural peat, organic soils and clays in the CKE trace reported by Hsi et al. (2005).

Table 4 – Variability of the consolidation parameters for different soil types in the CKR trace by Hsi et al. (2005)

Parameter	Soil type	Mean	Range
Coefficient of volume compressibility (m^2/MN)	**Peat**	**2.24**	**0.1 – 7.49**
	Organic	**1.20**	**0.2 – 3.70**
	Clay	**0.68**	**0.1 – 1.60**
Coefficient of consolidation (m^2/year)	**Peat**	**1.69**	**0.14 – 9.60**
	Organic	**1.57**	**0.27 – 8.80**
	Clay	**2.20**	**0.44 – 7.10**
Modified secondary compression index [$C_\alpha/(1 + e_0)$] (%)	**Peat**	**-**	**1.76 – 9.72**
	Organic soil	**-**	**1.97 – 4.06**
	Clay	**-**	**-**

The consolidation parameters vary over a wide range especially for peaty and organic soils. When considered together with the other uncertinities such as the layer thickness, loading intensity, and the accuracy of the analytical method used to model the consolidation process of the soft soils, there is a high degree of uncertainty over the preloading duration and the long term settlement prediction during the initial design stage.

4.0 Use of the observational approach to improve the initial design

In the observational approach, the performance of the road embankment during the construction stage is monitored to investigate any deviation of its behaviour from the initial design, which is based on the behaviour anticipated under the most probable conditions. The quantities to be observed during the construction stage should be selected and the probable limits of the variations of the measured parameters based on the working hypothesis should be established. If any deviation of the observed quantities from the expected range is noted the contingency plans should be put into operation to remedy the situation.

4.1 Use of the observational data to enhance the short term stability of road embankment

After deciding on the quantities to be observed, necessary instrumentation should be done. The quantities generally monitored to assess the short term stability of the road embankment are the vertical settlement, horizontal displacement and the excess pore pressure generation within the soft soil layer during loading. The vertical settlement of the embankment is monitored by installation of settlement plates and/or settlement pins while the horizontal displacement is monitored by installation of inclinometers and/or displacement stakes. Similarly, the pore pressure is monitored by installation of piezo-meters within the soft soil layers. The success of the observational approach depends very much on the reliability of the measured quantities, the speed of analysis and interpretation of the observed data and, if needed, the promptness of the remedial actions taken. The coordination between the field monitoring team, geotechnical analysis team and the construction team is of utter most importance in this process. Breakdown in the communication between the teams can result in disastrous consequences.

Matsuo and kawamura (1977) developed charts, given in Figure 4, for monitoring of stability of embankment on soft grounds based on the lateral displacement of the embankment (δ) and the vertical settlement (ρ_t) at the centre of the embankment. According to Matsuo and kawamura (1977) the settlement at the centre of the embankment is an index of the consolidation settlement and the lateral displacement of the embankment is an index of shear deformation. Matsuo and kawamura (1977) defines unstable slopes when the progress of the shear deformation is faster than the consolidation settlement. In addition to the above mentioned stability plots, other criteria such as settlement rate and displacement rate are also considered in assessing the stability of embankments on soft grounds.
If the observed FoS falls below the expected level, the construction plan should be changed to maintain the required level of safety. In this regards, filling rate is regulated so that the factor of safety is within allowable limits.

4.2 Use of the observational data to enhance the serviceability performance of the embankment

The preloading duration and the surcharge level of the embankment in the initial design may be based on some optimistic assessment of the consolidation characteristics of the soft soil. Therefore, the initial design should be checked against the actual performance of the embankment to ensure satisfactory serviceability state of the embankment. In this respect, prediction of the primary and secondary consolidation settlement of the embankment is important.

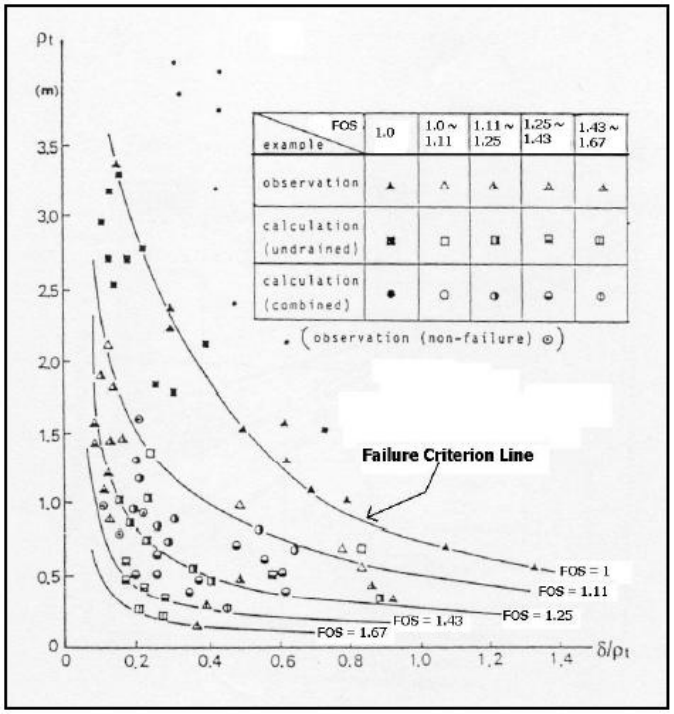

Figure 4 – Modified stability charts by Matsuo and Kawamura (1977).

4.2.1 Prediction of the primary consolidation settlement from the observed data

Asaoka (1978) proposed a method to estimate the total primary consolidation settlement from the measured settlement data. In his method, the time settlement plot is drawn and divided into equal time steps of Δt. The settlement at the end of the n^{th} time step S_n is plotted against settlement at the beginning of the n^{th} time step (S_{n-1}) as shown in Figure 5.

Then, a 45^0 line is drawn on the same plot and the settlement corresponding to the intersection point of the two lines is taken as the total primary consolidation settlement. Ariyaratna and Thilakasir (2010) showed that the Asaoka method can be used to accurately estimate the total primary consolidation settlement of Sri Lankan peaty soil.

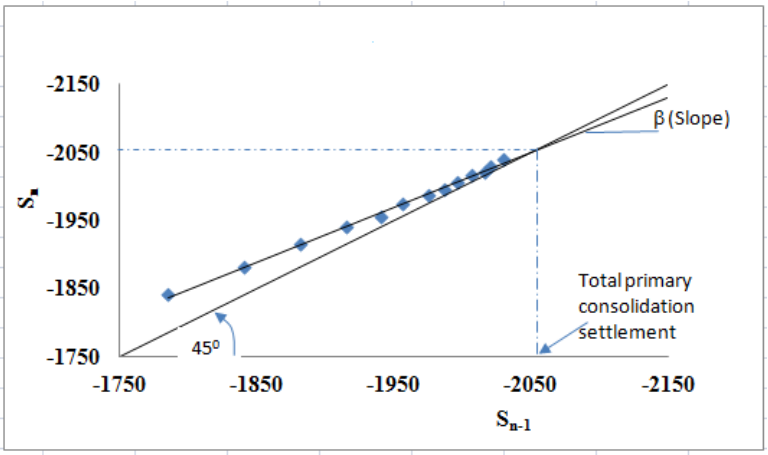

Figure 5 – Estimation of the total primary consolidation settlement using Asaoka (1978) method.

The estimated total primary consolidation settlement may be used to determine the degree of consolidation of the underlying soft layer and prediction of the time required to achieve 95% degree of consolidation. The slope β of the S_n vs, S_{n-1} plot may also be used to estimate the approximate coefficient of consolidation of the soft soil layer using the relationship given in Equation [2].

$$C_v = \frac{5}{12} h^2 ln \frac{\beta}{\Delta t} \qquad [2]$$

Where h is the thickness of the soft soil deposit.

The primary consolidation properties back analysed from the observed behaviour of the embankment should be compared with the same parameters used in the initial design and necessary adjustments to the initial design should be carried out.

4.2.2 Prediction of the secondary consolidation settlement from the observed data

Secondary consolidation settlement of peaty soil may continue well after the end of primary consolidation settlement and can cause serious maintenance issues during the service life of the embankment. Therefore, the secondary consolidation settlements should be limited to a predetermined value within a certain time period. For example in the CKE project, the settlement of the road embankment should be less than 154 mm within the defect liability period of two years after construction of the road pavement. Therefore, the observed settlement data may be used to reliably estimate the expected settlement during this time period. There are different methods available for the prediction of the long term secondary consolidation settlement and commonly used methods are the hyperbolic method and the log – time method.

4.2.2.1 Hyperbolic method

The resultant consolidation settlement is assumed to have a hyperbolic variation with time and according to this method the settlement (S) is related to the elapsed time (t) through Equation [3]

$$S = \frac{t}{\alpha t + \beta} \qquad [3]$$

Where α and β are constants.

The above equation may be rearranged to give Equation [4].

$$\frac{t}{S} = \alpha t + \beta \qquad [4]$$

The best fit straight line is plotted between the (*t/S*) vs. *t*, as shown in Figure 6 and the constants α and β are estimated from the slope and the intercept of the straight line variation. According to this method, the total final settlement is equal to $1/\alpha$. The estimated α and β values may be used to predict the settlement with time as shown in Figure 7.

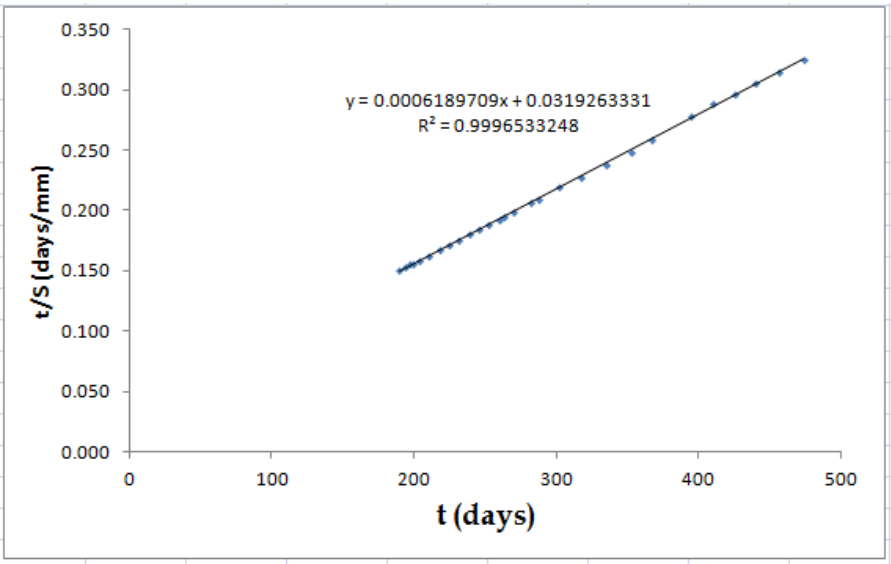

Figure 6 – Graph of (t/S) vs. t

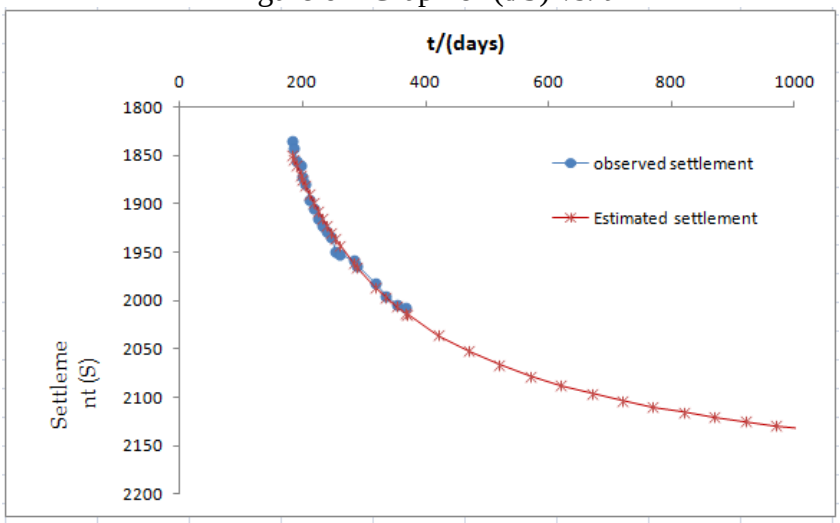

Figure 7 – Observed settlement and the predicted settlement with time.

The estimated α and β values may be used to predict the settlement during a certain time period after laying of the road pavement and the predicted settlement should be compared with the specified limit of the settlement for the same duration. The predicted settlement is 36 mm during the defect liability period of two years after placing of the road pavement and it is within the specified limit of 154mm.

4.2.2.2 Log – time method

Log-time method assumes that the variation of the secondary consolidation settlement (S_s) follows a linear variation with the log of the elapsed time and the secondary consolidation

starts after the end of primary consolidation settlement. The relationship between the secondary consolidation settlement (S_s) and the time (t) is expressed by Equation [5].

$$S_s = \frac{HC_\alpha}{1+e_0} log \left[\frac{t}{t_p}\right] \qquad [5]$$

Where H, C_α, e_0, and t_p are the thickness of the soft soil layer, coefficient of secondary compression, initial void ratio and the time taken for the end of primary consolidation settlement respectively.

At any given time after the end of primary consolidation settlement, the total settlement, S, is equal to the summation of the total primary consolidation settlement, S_p, and the secondary consolidation settlement, S_s, estimated from Equation [4]. The primary consolidation may be estimated using the Asaoka (1978) method and may be combined with the log-time method to predict the secondary consolidation settlement. The observed data is matched by varying the modified compression index $C_\alpha^{/} = C_\alpha/(1 + e_0)$ in Equation [4]. The obtained $C_\alpha^{/}$ value is used in the prediction of the long term secondary consolidation settlement.

The same observed settlement data, used in Figures 5 and 6 are used to predict the long term consolidation settlement using the log-time method. The observed settlement data and the matching estimated settlement data with $C_\alpha^{/}$ = 0.035 are shown in Figure 8. The value of the modified compression index is within the observed range given in Table 3. The predicted settlement during the defect liability period is 90 mm. It is interesting to note that the settlement predicted from the hyperbolic method during the same time period is 36mm.

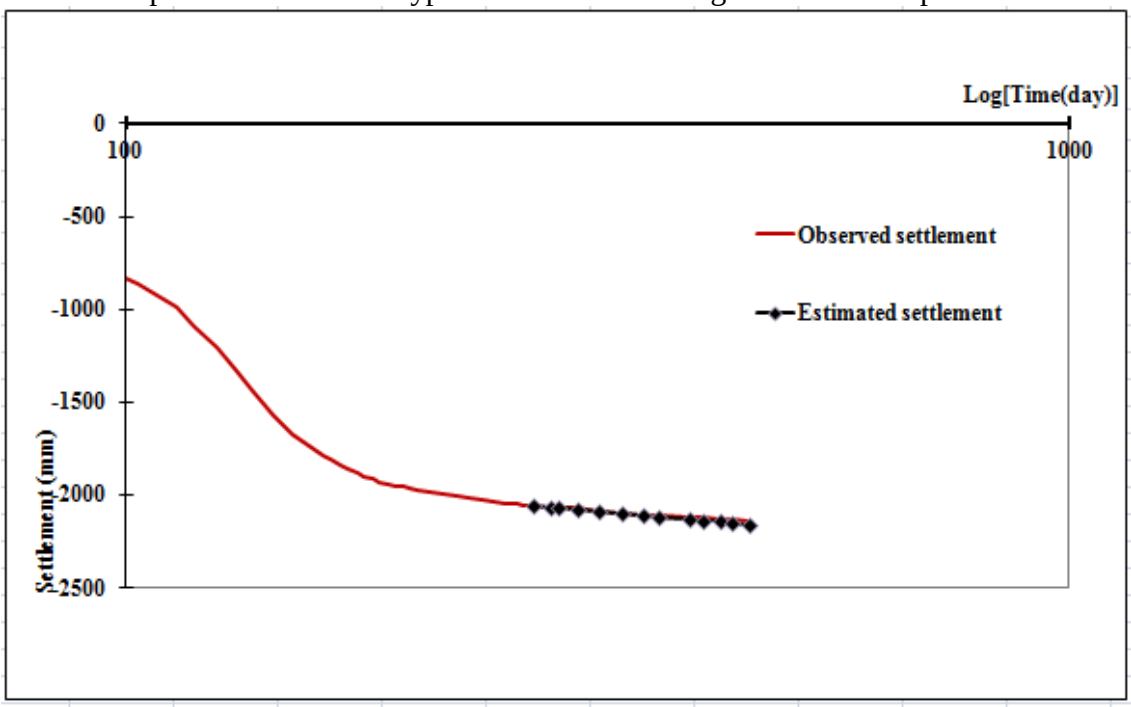

Figure 8 – Observed settlement and the matching settlement using log-time method.

Observed settlement monitoring data were used to predict the expected settlement during a two year period using the hyperbolic method and the log-time method. The predicted settlements are given in Table 5.

Table 5 - Settlement predicted from hyperbolic method and the log-time method during a time period of two years

Section	Location of the settlement plate	Predicted settlement (mm)		Section	Location of the settlement plate	Predicted settlement (mm)	
		Hyperbolic method	Log-time method			Hyperbolic method	Log-time method
Section 1	RHS	38	88	Section 7	RHS	31	95
	CL	31	88		CL	36	107
	LHS	33	96		LHS	48	125
Section 2	RHS	38	88	Section 8	RHS	44	95
	CL	No SP*	87		CL	No SP*	No SP*
	LHS	38	106		LHS	41	85
Section 3	RHS	33	83	Section 9	RHS	31	110
	CL	35	93		CL	28	110
	LHS	28	75		LHS	30	110
Section 4	RHS	39	88	Section 10	RHS	23	124
	CL	No SP*	No SP		CL	37	124
	LHS	36	96		LHS	19	107
Section 5	RHS	32	96	Section 11	RHS	26	90
	CL	36	90		CL	No SP*	No SP*
	LHS	39	108		LHS	23	90
Section 6	RHS	28	96	Section 12	RHS	20	75
	CL	No SP*	No SP		CL	56	150
	LHS	35	96		LHS	44	115

*No SP – No settlement plate

Based on the above estimation, the predicted settlement from the hyperbolic method is less than the same from the log-time method at all the sections considered. When one looks at the two methods, the log-time method has some credibility over the hyperbolic method as the material parameters of the log-time model can be obtained from laboratory testing. Furthermore, based on the results of the laboratory experiment, Mesri et al. (1997) had developed set of curves illustrating the dependency of the compression index C_α on the surcharging ration $R_s^{/} = (\sigma_{vs}^{/}/\sigma_{vf}^{/})$ - 1, where $\sigma_{vs}^{/}$ is the maximum effective vertical stress reach before removal of the surcharge and $\sigma_{vf}^{/}$ is the final effective vertical stress after removal of the surcharge. The ratio between the coefficient of secondary consolidation

after removal of the surcharge, $C_\alpha^{//}$, to the original coefficient of secondary consolidation, C_α, is related to $R_s^{/}$ depending on the (t/t_i) as shown in Figure 9. t_l is the elapsed time after removal of the surcharge at which the secondary consolidation reappears.

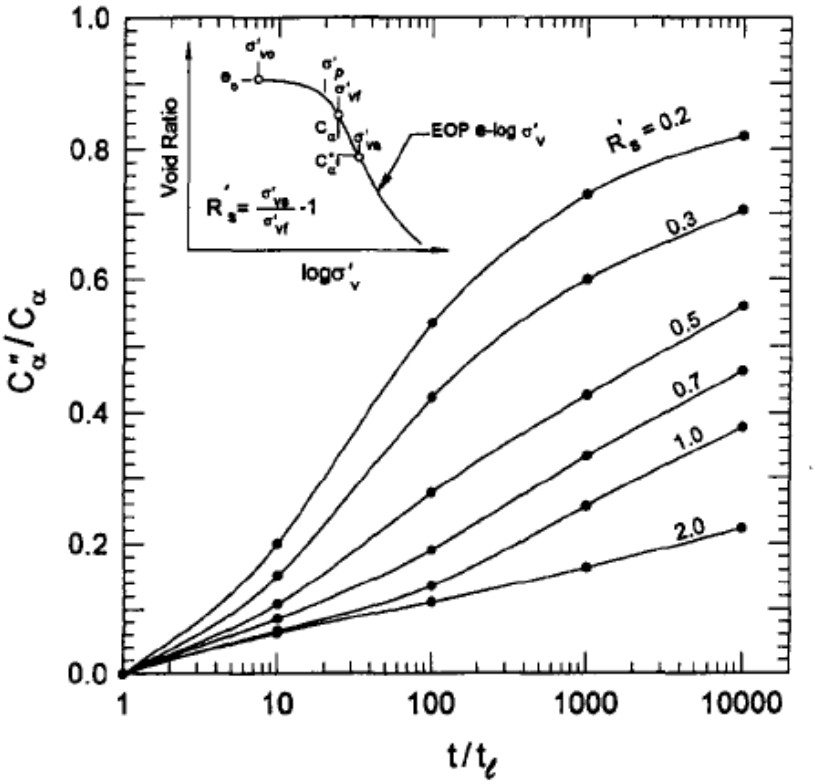

Figure 9 – variation of $C_\alpha^{//}/C_\alpha$ with $R_s^{/}$ and t/t_i.

When the log-time method is used in the prediction of the secondary consolidation settlement, effects of the surcharging can also be incorporated in to the settlement prediction procedure. Moreover, the settlement predicted from the log-time method is a conservative estimate of the expected settlement. Therefore, the log-time method may be preferred over the hyperbolic method in the estimation of the long term secondary consolidation settlement.

5.0 Conclusions

Uncertainties associated with the design of road embankments over soft soil deposits in Sri Lanka are highlighted using the material properties reported in the literature. In this context, the importance of using the observational approach in the construction of embankment over the soft soil deposits is illustrated. Particular attention was paid to the effects of using the most probable conditions in the initial design. It is shown that depending on the financial and time restrictions of individual projects, soil properties used in the initial design may be varied. If the project has tight financial and time restraints, the material parameters may be taken closer to the most prismatic values and the design will become more or less a conventional design.

Use of the observational method in enhancing the short term stability and the long term serviceability condition of the road embankments constructed over soft soil deposits are presented. Particular attention was paid to the use of hyperbolic method and the log-time method in the prediction of the secondary consolidation settlement. It was shown that the secondary consolidation settlement predicted from the log-time method is generally more than the same estimated using the hyperbolic method. Moreover, the use of the log-time method in prediction of the secondary consolidation settlement considering the effects of surcharging was also discussed.

References

1. Ariyarathna, P.R.C. and Thilakasiri, H. S., 2011, “Improvement of Sri Lankan Peaty Soil by Vacuum Consolidation”, Proc. Asian Regional Conference, ISSMGE, Hong kong.
2. Asaoka, A., 1978, “Observational procedure of settlement prediction”, Soils and Foundations, 18(4), pp 87 – 101.
3. BSI (2004). Eurocode 7: Geotechnical design – Part 1: General rules. BS EN 1997-1:2004, British Standards Institution, London.
4. Hsi, J., Gunasekara, G., and Nguyen, V, 2005, “Characteristics of soft peat, organic soils and clays, Colombo – Katunayake \Expressway, Sri Lanka, Ground Improvement Case studies, Ed: Indrarathne, B, and Chu, J., Vol.3, Elsevier.
5. Matsuo, M., and Kawamura, K., 1977, “Diagram for construction control of embankment on soft ground”, Vol. 17, No. 3 pp:37 – 52.
6. Mesri, G., Stark, D., Ajlouni, M. A., and Chen, C. S., 1977,“Secondary compression of peat with or without surcgaring”, J. Geotechnical and Geo-environmental engineering, vol. 123, 5, May.
7. Peck, R. B., 1969, “Advantages and limitations of the observational method in applied soil mechanics”, Géotechnique, 19 (2), pp:171-187.
8. Terzaghi, K., Peck, R. B., 1967, Soil mechanics in Engineering Practice. John Wiley, New York.